Electromagnetics Laboratory
Department of Electrical Engineering
University of Colorado, Boulder, Colorado 80302

MICROWAVE MODEL STUDY OF OPTICAL DIELECTRIC SLAB WAVEGUIDE†

By

H. A. Haddad, S. W. Maley and D. C. Chang

March, 1975

Scientific Report No. 12 (AFOSR-72-2417)

Prepared for
Air Force Office of Scientific Research (AFSC)
United States Air Force
Arlington, Virginia 22209

†This research was supported by the Air Force Office of Scientific Research (AFSC) under grant no. AFOSR-72-2417.

ABSTRACT

The objective of this work is to investigate the characteristics of dielectric slab waveguides frequently used in integrated optics by a microwave modeling technique. The study includes excitation of a surface wave mode in a low loss dielectric waveguide as well as coupling between two similar (degenerate mode) and different (non-degenerate) waveguides. The experimental data indicate the coupling length is short for the non-degenerate, and decreases as the separation between the two guides decreases for either case (degenerate or non-degenerate).

We also investigated the field characteristics outside a curved slab and the containment of radiation. Previous theoretical work indicated that the use of $1/\rho$ type profile in the refractive index would reduce the radiation losses. Unfortunately, such a graded profile cannot be obtained physically. A simple solution is to truncate the inverse-linear profile at some finite distance from the guide to achieve a substantial reduction of radiation. Experimentally, we achieved a tapered profile by using a triangular taper. This resulted in reducing the radiation by as much as 3 db over the untapered case.

Also included in this work is the investigation of far field pattern for guides with different radii of curvature.

ACKNOWLEDGEMENTS

We wish to thank Professor L. Lewin, Professor F. Barnes and E. F. Kuester for numerous discussions. Also, the authors are indebted to Mrs. Marie Kindgren, Mrs. Eleanore Schofield and Ms. Ann Worrell for their preparation of the manuscript. We would like to thank Mr. Kawan Al-Ani for preparation of the drawings.

This research was supported by the Air Force Office of Scientific Research (AFSC) under grant no. AFOSR-72-2417.

TABLE OF CONTENTS

LIST OF FIGURES

CHAPTER I

INTRODUCTION

Studies of surface wave modes were made as early as 1907 by Zenneck who considered a plane wave incident on a lossy dielectric medium. But serious practical use of this type of mode for communication was made in the fifties when Gaubau [24] suggested the use of a dielectric-coated single conductor surface-wave transmission line. Theoretical analysis of these so-called G-lines were made by Barlaw and Cullen [25], for individual lines and by Meyerhoff [26], among others, for the coupling between two surface wave transmission lines (Gaubau lines). Also, Cullen [27] analyzed, theoretically, the surface wave excitation of a single dielectric slab waveguide. Due to the intrinsic losses of these G-lines the practical use of them is restricted to mainly microwave application. More recently there has been considerable research in surface wave propagation along pure dielectric waveguide structures. Some of the interest was in fiber optics for long distance communication [1], other in integrated optics [2]. The losses of fiber lines were reduced drastically to a few decibels per kilometer so that the use of fibers for optical communication becomes more of a reality. Meanwhile progress made in optical fibers also opens the way in the design of small components devices called "integrated optics," where active and passive devices can be built on a common substrate and connected to a dielectric waveguide [32].

Snitzer [28] reported some experimental studies of several low-order modes that appeared alone or in a combination on fiber waveguides. The theory of higher-order hybrid modes of dielectric guides was advanced by Snitzer [29] and Kapany and Burke [30]. A theoretical study of the launching of $HE_{1,m}$ modes by plane wave with the wave vector parallel to the axis of a circular rod was reported by Snyder [31]. Optical guides radiate energy from bends. Marcattili [15] and Lewin [17] formulated a closed form expression for the attenuation due to these bends. Chang and Barnes [11] treated the reduction of radiation from bends for a curved dielectric slab. Maley [12] found the far field pattern and the radiated power due to the discontinuity from straight into curved slab waveguides. Jones [14], Arnaud [13] and Kuester and Chang [8] analyzed coupling phenomena between two dielectric waveguides for degenerate and non-degenerate surface wave mode.

Up to now there has been little experimental investigation of the coupling and radiation losses in dielectric waveguides (fibers or slab waveguides). At optical frequencies detailed study of these structures is hampered by their small size of the order 10-50 microns. In order to circumvent this difficulty, we investigated in this report a microwave scale model of these optical dielectric waveguides. This can be done using microwave frequency since uniformity, surface roughness and dimension of the waveguides can be controlled with precision. In addition, the possibility of minimizing the radiation from bends and coupling between two waveguides could be studied

experimentally.

In this investigation a dielectric slab waveguide having small relative dielectric constant $\varepsilon_r = 1.03$) was simulated using a microwave model. The waveguide was designed to support just a single mode (TE_o) and the thickness was about 9.2 cm, where the frequency of operation is 9 GHz.

Chapter III deals with the experimental setup being used for the excitation of a surface wave model. Also, the design of a single mode dielectric slab waveguide is treated there. Chapter IV is devoted to the experimental and theoretical investigation of a single mode slab waveguide. Coupling between two dielectric slab waveguides for degenerate and non-degenerate cases was presented in Chapter V. A theoretical analysis was included also. However, Chapter VI mainly treats, experimentally, the radiation due to bends in slab waveguides. Reduction of radiation and far field pattern are discussed. Results of this study as well as some suggestions are summarized in Chapter VII. The Appendix contains some Basic-Computer Programs for the solution of transcedental mode equations, the magnitude and phase of the coupled system modes, and attenuation and radiation losses from curved guides.

This work is mainly experimental in nature, although some theoretical justification is included.

CHAPTER II

THEORY

In this chapter, we first summarize some of the known theoretical results pertinent to our investigation.

(a) Single Slab Waveguide

A surface wave mode can be guided along a dielectric slab waveguide. These modes have an evanescent character in the outside region of the slab due to the unboundedness of these structures. In general surface wave modes in a symmetric slab have the following characteristics:

1. No low frequency cutoff for the dominant mode.
2. A finite number of discrete modes of propagation at a given frequency.
3. The possibility of a mode solution with a phase velocity less than the speed of light in free space.

Inside the dielectric slab region these modes can be considered as a plane wave incident from the dielectric region onto the air-dielectric interface at an angle less or greater (depending on how the angle is measured) than the critical angle θ_c where $\sin \theta_c = \frac{1}{n_1}$ and n_1 is the refractive index of the dielectric slab. For incident angles greater than the critical angle there is complete reflection at the interface and the field outside the dielectric is evanescent type.

Therefore the plane waves propagate in a zigzag path along the z axis undergoing complete reflection at each interface.

For a two dimensional dielectric slab waveguide with air in the outside region and for a TE type excitation the wave equation renders two types of modes (even and odd) as given in [6-7]. Assuming no variation along y direction,

$$\frac{\partial}{\partial y} = 0 \qquad (2\text{-}1)$$

and with time and z dependence of the form

$$e^{i(\omega t - \beta z)} \qquad (2\text{-}2)$$

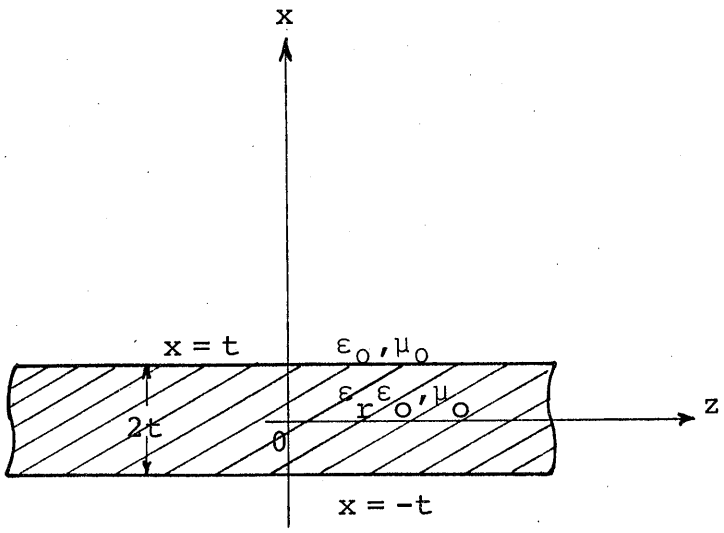

Fig. 1: Single Slab Dielectric Waveguide

we have for the even guided modes, a field distribution of

$$E_y = A_e \cos hx \qquad |x| < t \tag{2-3}$$

$$H_z = -\frac{ih}{\omega\mu_o} A_e \sin hx \tag{2-4}$$

where

$$h^2 = n_1^2 k_o^2 - \beta^2 \tag{2-5}$$

$$E_y = A_e \cos ht \; e^{-p(|x|-t)} \qquad |x| > t \tag{2-6}$$

$$H_z = -\frac{x}{|x|}\frac{ip}{\omega\mu_o} A_e \cos ht \; e^{-p(|x|-t)} \tag{2-7}$$

and

$$p^2 = \beta^2 - k_o^2 \tag{2-8}$$

where h is the transverse propagation constant inside the slab region,

p is the decay constant outside the slab.

β is the propagation constant along the z axis.

t half width of the slab

$n_1 = \varepsilon_r^{\frac{1}{2}}$ is the refractive index inside the slab.

$k_o = \frac{2\pi}{\lambda}$ is the free space propagation constant.

The significance of the above equations is the evanescent field character in the outside region and the slow character of the wave along the z axis. The surface wave phase velocity

$$v_z = \frac{\omega}{\beta} = \frac{ck_o}{\beta} \tag{2-9}$$

is therefore slower than c, the velocity of light in air. Therefore these structures are often referred to as slow-wave structures. In the above analysis the requirement for a mode to be guided is that $p^2 > 0$.

An eigenvalue equation for finding h and p can be found by applying boundary conditions. These equations are given by:

$$\tan ht = \frac{pt}{ht} \tag{2-10}$$

and

$$(pt)^2 + (ht)^2 = (n_1^2 - 1)(k_o t)^2 \tag{2-11}$$

The solution of the above equations (which can be put into one trancendental equation) will determine the character of the field inside and outside the slab surface, also the velocity that the wave propagates along the z axis. The power P flowing in the z direction per unit length in the y direction is given by

$$P = \frac{1}{2}\int_{-\infty}^{\infty} \mathrm{Re}(\bar{E} \times \bar{H}^*) \cdot dS = \frac{\beta}{\omega\mu_o} |E_y|^2 dx \tag{2-12}$$

or

$$P = \left(\frac{\beta t + \beta/p}{2\omega\mu_o}\right) A_e^2 \tag{2-13}$$

The significance of equation (2-13) is that the amplitude of the field A_e can be found in terms of the power P flowing in the z direction.

The odd mode type solution is given as

$$E_y = A_o \sin hx \qquad |x| < t \qquad (2\text{-}14)$$

$$E_y = \frac{x}{|x|} A_o \sin ht \; e^{-p(|x|-t)} \qquad |x| > t \qquad (2\text{-}15)$$

and its eigenvalue equation is

$$\cot ht = - \frac{pt}{ht} \qquad (2\text{-}16)$$

Therefore depending on the physical dimension of the slab, its refractive index and the frequency of operation, a single mode or multimode waveguide can be designed. It is obvious from equation (2-10) that the lowest order mode has no lower cutoff frequency. Also at a specific frequency there is only finite number of propatating modes.

Radiation modes can also exist in a slab waveguide. These unguided modes come out as a solution of the wave equation and satisfy Maxwell equations, if we consider a plane wave incident from the outside region onto the slab waveguide. As a result of the refraction and reflection, a standing wave can exist inside and outside the slab surface. These modes do not decay in the outside region and are bound to the dielectric waveguide. The normalization of these modes involves a delta function [20]. Marcuse [6] presented detailed information about these radiation modes.

(b) Coupling Between Two Dielectric Waveguides:

There exist many theoretical papers concerning this subject. Marcuse [4] obtained the coupling coefficient of two parallel dielectric waveguides of arbitrary shape and arbitrary distribution of refractive index using perturbation theory. His result applies only to degenerate modes (modes having equal phase velocities). Jones [14] using dyadic Green's functions, found the coupling coefficient between two parallel (arbitrarily) shaped waveguides that includes the effect of continuous mode spectrum,
There is a large amount of literature on this subject. Kuester and Chang [8] give comprehensive discussions on this topic. They also treat the coupling problem by using a variational technique. This method renders a far better esult than the above mentioned papers especially in the non-degenerate case and for a very closely spaced waveguide. The following results were obtained from their paper.

Continuous coupling between two parallel dielectric waveguides will occur due to the evanescent nature of the surface-wave modes in the region outside of the waveguide. In Fig. 2 a cross-sectional view of two waveguides is shown. Each of the two guides has a refractive index profile of $(n_i^2 + n_3^2)^{\frac{1}{2}}$ where $i = 1$ or 2 and n_3 is the refractive index of the surrounding medium. Assuming that the separation between the two guides is very large, the system field can

be given as

$$\bar{E}^{+} = m_1 \bar{E}_1^{+} + m_2 \bar{E}_2^{+}$$
$$\bar{H}^{+} = m_1 \bar{E}_1^{+} + m_2 \bar{H}_2^{+} \qquad (2\text{-}17)$$

where $(\bar{E}_{1,2}^{+}\ \bar{H}_{1,2}^{+})$ are the transverse field distributions for the two waveguides, each in the absence of the other, for propagation in the forward z-direction with propagation constant $\beta_{1,2}$. m_1 and m_2 are as yet undetermined constants. By using a variational formulation and the application of the Rayleigh-Ritz principle, it was found that the system propagation constant β could be written as

$$\beta_{\pm} = \beta_{av} \pm \Delta\beta \qquad (2\text{-}18)$$

where

$$\beta_{av} = \frac{1}{2}(\beta_1 + \beta_2)$$

and

$$\Delta\beta = \sqrt{\Delta^2 + \delta^2} \qquad (2\text{-}19)$$
$$\Delta = \frac{1}{2}(\beta_1 - \beta_2)$$

$$\delta^2 = c_1 c_2 / P_1 P_2 \qquad (2\text{-}20)$$

where

$$P_{1,2} = 2 \int [\bar{E}_{t1,2}^{+} \times \bar{H}_{t1,2}^{+}] \cdot \bar{a}_z dS \qquad (2\text{-}21)$$

$$C_{1,2} = \omega \varepsilon_o \int \varepsilon_{1,2}\ \bar{E}_1^{+} \cdot \bar{E}_2^{-}\ dS \qquad (2\text{-}22)$$

Here the surface integration is over the entire cross-sectional plane; (μ,ε) are the permeability and permittivity

of the dielectric media; $\bar{E}^{\pm} = E_z^{\pm}\,\bar{a}_z + \bar{E}_t^{\pm}$ so that $\bar{E}_t^{\pm}$, $\bar{E}_z^{\pm}$ are the transverse and longitudinal components of $\bar{E}^{\pm}$ respectively. $(\bar{E}^-, \bar{H}^-)$ is the "adjoint" field of $(\bar{E}^+, \bar{H}^+)$ having a transverse field distribution,

$$\bar{E}_t^- = \bar{E}_t^+ , \quad E_z^- = -E_z^+ ; \quad \bar{H}_t^- = -\bar{H}_t^+, \quad H_z^- = H_z^+ \tag{2-23}$$

and propagating in the negative z-direction. It is clear that $P_{1,2}$ are associated with the power flow of the two individual waveguides, and $C_{1,2}$ are associated with the mutual coupling of power between the two guides. $C_{1,2}$ are expected to be much smaller than $P_{1,2}$ since $C_{1,2}$ involves only surface integration over the individual waveguide cross sections where the field of the other waveguide is exponentially small. Hence from (2-18), there exist two waveguide system modes whose propagation constants β_+ and β_- are centered at $(\beta_1 + \beta_2)/2$ and separated from each other by the amount of $2\Delta\beta$. The transverse field distribution of these two system modes are given by

$$\bar{E}^+ = m_1(\bar{E}_1^+ + q_{\pm}\,\bar{E}_2^+) \tag{2-24}$$

where

$$q_{\pm} \simeq \sqrt{\frac{P_1}{P_2}}\left[\frac{-\Delta \pm \sqrt{\Delta^2+\delta^2}}{\delta}\right] \tag{2-25}$$

In the case of coupling between two degenerate modes in a system of two identical waveguides $\beta_1 = \beta_2$, this implies

$q = 1$. Hence one of the system modes is symmetrical, $\bar{E}_s^+ = \bar{E}_1^+ + \bar{E}_2^+$ while the other is antisymmetrical $\bar{E}_a^+ = \bar{E}_1^+ - \bar{E}_2^+$.

If a surface-wave mode initially propagates in only one of the two identical lossless dielectric waveguides, i.e. $\bar{E}_2^+(z = 0) = 0$. The total field at $z = 0$ would be two system modes of equal amplitudes

$$\bar{E}_{t_o t.}^+ = \bar{E}_s^+ + \bar{E}_a^+ \tag{2-26}$$

Since the symmetric and anti-symmetric modes have different phase velocity, they interfere with each other either constructively or destructively according to

$$\bar{E}_{t_o t}^+ = \bar{E}_s^+ e^{-i\beta_+ z} + \bar{E}_a^+ e^{-i\beta_- z} \tag{2-27}$$

as shown in Fig. 3 for two identical slab waveguides. At a distance L (called the coupling length),

$$L = \frac{\pi}{(\beta_+ - \beta_-)} = \frac{\pi}{2\Delta\beta} \tag{2-28}$$

the two amplitudes become equal but opposite. Hence at $z = L$ the total field corresponds to that of the surface-wave mode of an isolated second waveguide while the field in the first guide is identically zero. Thus there is a complete power transfer from guie 1 to guide 2 at $z = L$.

It was found for identical slab waveguides separated by distance d that $\Delta\beta$ is given by:

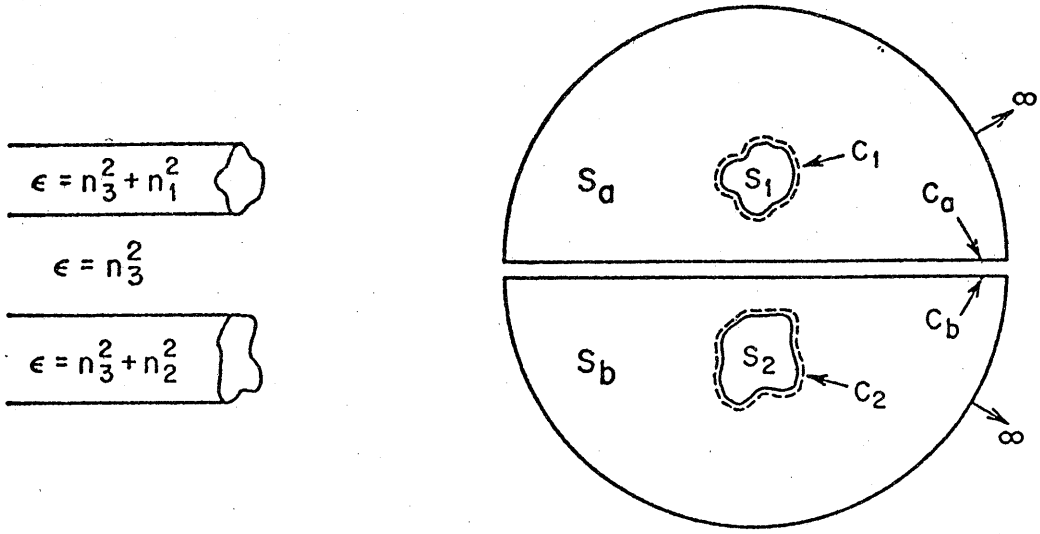

Fig. 2 Geometry of two parallel guides

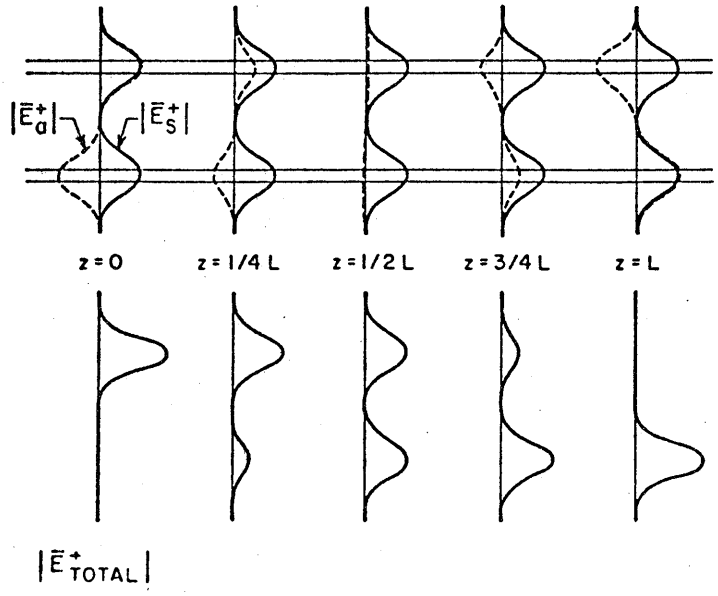

Fig. 3 Change in relative phase of E_a^+ and E_s^+ causes total field to transfer from guide 1 to guide 2

$$\Delta\beta = 2\,\frac{ph^2\, e^{-pd}}{k_o^2\beta_1(n_1^2-1)L_e} \tag{2-29}$$

where $L_e = D + 2/p$ and p,h and n_1 are given in part (a) of this chapter and D is the width of the slab. It can be seen from equation (2-29) that $\Delta\beta$ decreases exponentially for increasing the separation d.

In the case of non-degenerate modes, there is a partial transfer of power in comparison to a complete power transfer in the degenerate case whenever the coupling length is an integral multiple of L. The reason is that the two system modes are neither symmetrical or antisymmetrical. In this case the total electric field can be written as

$$\bar{E}^+_{t_o t} = \left(\frac{q_-}{q_- - q_+}\right)\bar{E}^+_{s+}\, e^{-i\beta_+ z} + \left(\frac{-q_+}{q_- - q_+}\right)\bar{E}^+_{s-}\, e^{-\beta_- z} \tag{2-30}$$

where

$$\bar{E}^+_{s\pm} = \bar{E}^+_1 + q_\pm \bar{E}^+_2 \,.$$

Also the maximum amount of power which can be transferred is given by

$$|S_{12}|^2 = \left|\frac{P_1}{P_2}\right| \frac{|\delta|^2}{|\Delta^2 + \delta^2|} \tag{2-31}$$

where for a lossless case

$$\left|\frac{P_1}{P_2}\right| \simeq 1$$

In conclusion the amount of coupling between modes in two parallel waveguides is very small except when the propagation constants of the two individual modes are nearly equal, $\beta_1 = \beta_2$.

(c) Radiation from Bends:

Considerable research has been made in this area. Marcatili [15], formulated the problem in terms of cylindrical functions with some approximations to the characteristic equation. Lewin [17] treated the problem of bends in fiber using toroidal structure. He built up an integral formulation for the field which satisfies the Helmholtz equation and which is suitable in the toroidal system. However, Chang and Barnes [11], by using a suitable transformation, replaced a smoothly curved, homogeneous slab by a straight one with varying refractive index profile. Their technique was extended to bends in fibers. The formulations that will be presented in this section have been taken from the paper by Chang and Barnes.

By assuming that the field around the bend for TE-type surface mode with no variation along the y-direction is given by

$$E_y(\rho,\theta) = \Omega(\rho)e^{-ik\nu R\theta} \qquad (2\text{-}32)$$

where ν is the normalized propagation constant along the

azimuthal direction.

$k = \omega\sqrt{\mu_o \varepsilon_o}$ is the free space propagation constant.

$\Omega(\rho)$ is the transverse variation of the electric field.

R is the radius of curvature to the inner side of the curved slab.

Also by using a proper transformation

$$x = R \ln \rho/R \tag{2-33}$$

and

$$z = R\theta$$

The wave equation in curved coordinate was transformed into the following form

$$\frac{d^2\Omega}{dx^2}(x) + k^2[n_j^2 \exp(2x/R) - \nu^2]\ \Omega(x) = 0 \tag{2-34}$$

$$n_j = \begin{cases} n & \text{refractive index inside the slab} \\ 1 & \text{outside the slab} \end{cases}$$

The boundaries in this coordinate system are located at $x = 0$ and d where $d = R \ln(1 + D/R) \simeq D$.

As depicted in Fig. 4 a smoothly curved homogenous slab was replaced by a straight one which has approximately the same thickness, but with a varying refractive index profile. It is interesting to note from equation (2-34) that for fixed $\nu = \nu_o$ the term $\exp(2x/R) - \nu_o^2$ is real and negative near the slab surface but is real and positive for large x.

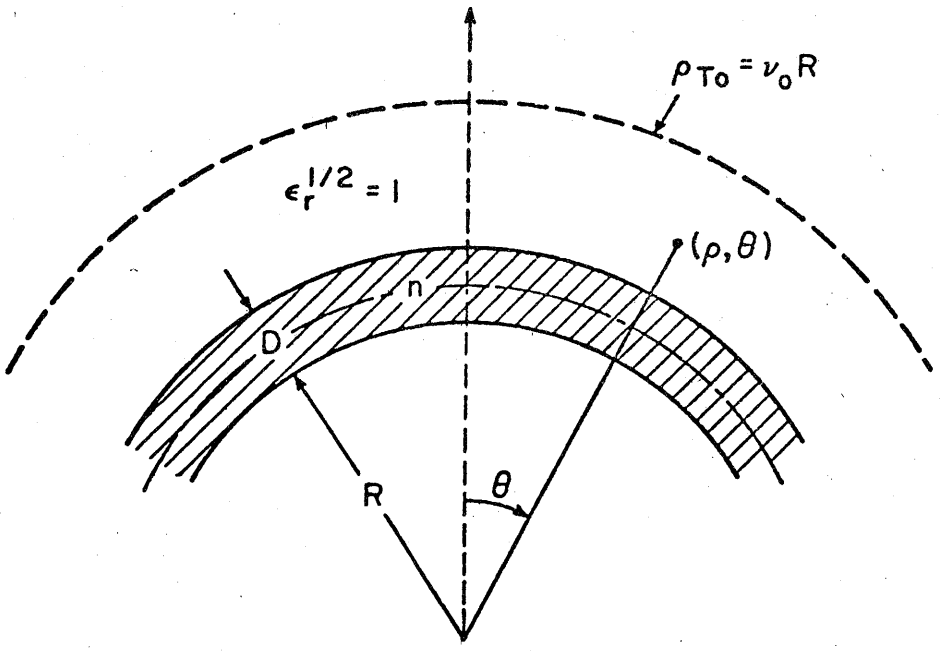

(a)

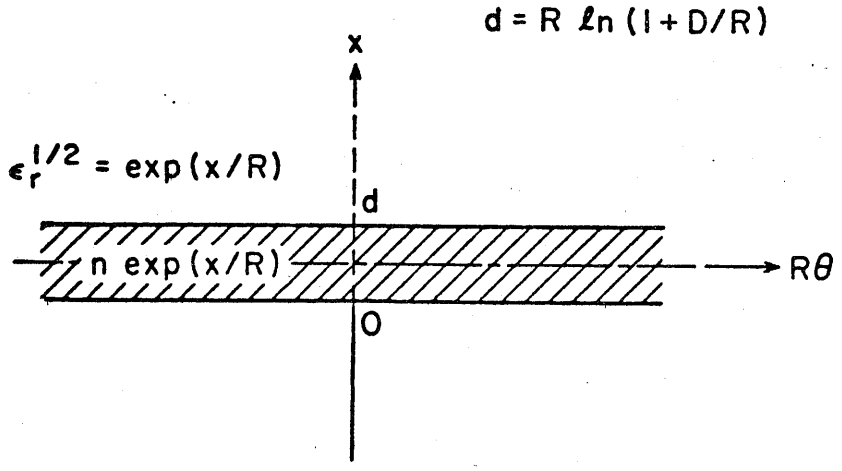

(b)

Fig. 4:

(a) Section of curved slab: geometry

(b) Equivalent straight slab.

At $x_o = R \ell n \nu_o$ or

$$\rho_o = \nu_o R \tag{2-35}$$

a turning-point will occur. Beyond this point, the solution would be in the form of an outgoing unattenuated wave so that the radiation condition at infinity will be satisfied. Suitable solution to (2-34) for inside and outside the slab were made using a WKB approximation and with the application of boundary conditions it was found that

$$e^{-ik\nu R\theta} = e^{-\alpha R\theta - ik\nu_o(R+D/2)\theta} \tag{2-36}$$

where

$$\alpha = \frac{\lambda_o \mu_o^2}{(n^2-1)\nu_o L_e} e^{-2\lambda_o^3 k_o R/3\nu_o^2} \tag{2-37}$$

and

$$L_e = D + 2/(k\lambda_o)$$
$$\lambda_o = (\nu_o^2 - 1)^{\frac{1}{2}}$$
$$\mu_o = (n^2 - \nu_o^2)^{\frac{1}{2}}$$

$\nu_o = \frac{\beta}{k_o}$ is the normalized propagation constant of a straight homogenous slab waveguide

$\mu_o = \frac{h}{k_o}$ is the normalized transverse propagation constant inside a straight homogenous slab.

$\lambda_o = \frac{p}{k_o}$ is the normalized decay constant in the outside region of a straight slab.

α is the attenuation constant.

p and h can be found from equations (2-10) and (2-11).

An interesting conclusion can be drawn from eq. (2-37); that is the attenuation per unit length α around a smoothly-curved guide is exponentially proportional to R. Hence the amount of attenuation can vary from negligibly small to very large over small range of R. Another conclusion that can be drawn from (2-37) is that for a fixed radius of curvature, a substantial reduction in attenuation can be achieved by decreasing the attenuation depth $p^{-1} = (k\lambda_o)^{-1}$ of the evanescent field. In other words the turning-point is being moved away from the slab.

It is clear that if radiation to be reduced, the turning point has to be relocated. A complete removal of this point (therefore, the radiation) will be possible if the refractive index of the surrounding material is changed to compensate the index variation due to curvature. The ideal profile for the refractive index would be of the form R/ρ. But unfortunately this kind of graded index profile is not physically acceptable because it requires the refractive index to vanish at infinity. A practical form is to truncate the inverse-linear profile at some finite distance so that the turning-point can be reasonably relocated.

(d) Radiation from a Circular Bend Between Two Discontinuities.

S. Maley [12], had solved this problem by assuming that the radius of curvature is sufficiently large so that the radiated power is small compared to the power carried by the waveguide. This provides a further assumption that the electromagnetic field inside the curved slab propagates around the bend essentially unchanged with respect to the straight guide. As depicted in Fig. 5, the assumption is that the incident transverse electric field for TE modes in the three regions are given by

$$\bar{E}_i = \bar{a}_x E_i \, e^{-i\nu_o kz}$$

$$\bar{H}_{it} = \bar{a}_z H_{iz} \, e^{-i\nu_o kz} \qquad (2\text{-}38)$$

in region 1

$$\bar{E}_i = \bar{a}_x E_i \, e^{-i\nu kr\phi}$$

$$\bar{H}_{it} = (-\bar{a}_y \sin\phi + \bar{a}_z \cos\phi) H i_z e^{-i\nu kr\phi} \qquad (2\text{-}39)$$

in region 2 where $0 \leq \phi \leq \psi$ and

$$\bar{E}_i = \bar{a}_x E_i \; e^{-i\nu kr\psi} \; e^{-i\nu_o kz'}$$

$$\bar{H}_{it} = (-\bar{a}_y \sin\psi + \bar{a}_z \cos\psi) H_{iz} \, e^{-i\nu k_o r\psi} e^{-i\nu_o kz'} \qquad (2\text{-}40)$$

in region 3, where $(\bar{E}_i, \bar{H}_{it})$ are the incident transverse electric and magnetic fields respectively. Power was assumed to flow from region 1 through region 2 into region 3.

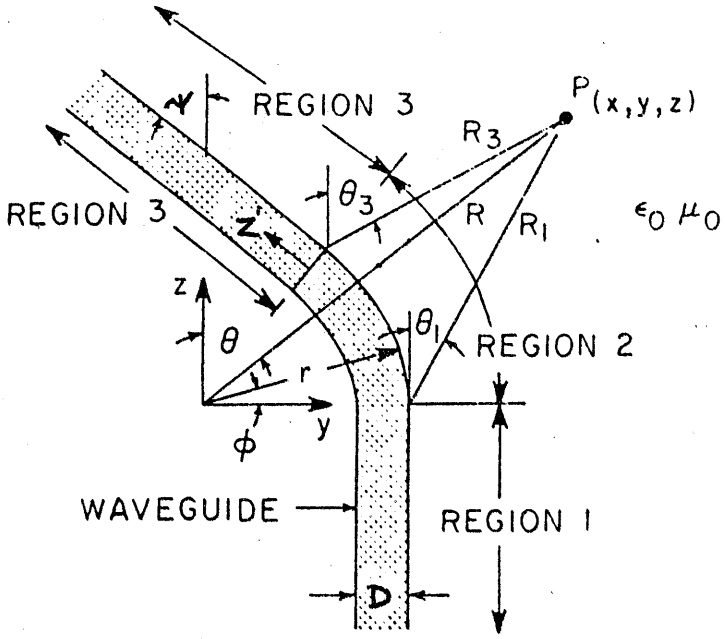

Fig. 5 Configuration of Dielectric Slab Waveguide

$E_i = A_e \cos ht$

$H_{it} = -i \frac{h}{\omega\mu_o} A_e \sin ht$

z' is the distance along the outer surface of the waveguide region 3.

$h = \sqrt{n^2 - \nu_o^2}\, k$ is the transverse propagation constant for a straight slab.

$k = \omega\sqrt{\mu_o \varepsilon_o}$ is the free space propagation constant.

$t = D/2$ is the half width of the slab.

ψ is the angle formed between the two straight sections.

$r = R + D$ is the radius of curvature to the outside region of the curved slab.

ν_o is the normalized propagation constant as given in part C of this chapter.

The main purpose of this assumption is to find the far field pattern of the electric field and the power lost in the outside region due to the discontinuity between the straight into curved section. As shown in Fig. 5, coordinates R_3 and θ_3 and coordinates R_1 and θ_1 gives the position of point P with respect to the upper and lower ends of the outer surface of the waveguide bend. It is assumed R, R_1 and R_3 are very large that they become nearly parallel. Using Jordan's notation, the magnetic and electric potential in the three regions can be expressed in terms of the electric and magnetic

current sheets, $\bar{J}$ and $\bar{M}$ respectively where

$$\bar{J} = \bar{n} \times \bar{H}_{it}$$
$$\bar{M} = -\bar{n} \times \bar{E}_{i}$$

and $\bar{n}$ is the outward normal vector.

These complicated integral expressions are evaluated using different asymptotic techniques to give the magnetic and vector potentials $\bar{A}$ & $\bar{F}$. The electric and magnetic fields are then found from

$$\bar{E} = -i\omega\mu\bar{A} - \nabla \times \bar{F}$$
$$\bar{H} = \frac{i}{\omega\mu} \nabla \times \bar{E} \qquad (2\text{-}41)$$

Thus

$$\bar{E} = -\bar{a}_x MG(\theta)$$
$$\bar{H} = -\frac{M}{\eta_o}[\bar{a}_y \cos\theta - \bar{a}_z \sin\theta]G(\theta) \qquad (2\text{-}42)$$

where

$$G(\theta) = (Y-\sin\theta)e^{ikr\sin\theta} f(\theta) - (Y-\sin(\theta+\psi)) \cdot e^{-ikr\nu\psi} e^{ikr\sin(\theta+\psi)} f(\theta+\psi) \qquad (2\text{-}43)$$

and

$$M = \frac{(1+i)e^{-ikR_o} E_i}{4(\pi k R_o)^{\frac{1}{2}}}$$

$$Y = \frac{\eta_o H_{iz}}{E_i} = -ih\tan ht \quad .$$

Also

$$f(\Phi) = \frac{1}{\nu_o - \cos\Phi} - \frac{1}{\nu - \cos\Phi} \qquad (2\text{-}44)$$

where Φ either θ or $\theta + \psi$

and $\eta_o = \sqrt{\frac{\mu_o}{\varepsilon_o}}$ is the free space wave impedance.

It is important to note that if the phase distribution of the waves is uniform along the entire waveguide ($\nu = \nu_o$), then there is no radiation. However for a curved structure ν is very close to ν_o but not equal (refer to part C of this Chapter). Thus from equations (2-44) and (2-42), $\bar{E}$ and $\bar{H}$ are both very sensitive to the value of ν and ν_o.

An approximate value for the number, N, of lobes between the vertical and the waveguide was derived by analyzing the rapidly varying term in $G(\theta)$ of the electric field $\bar{E}$. This number of lobes is given by

$$N \cong \frac{4 k_o r}{\pi} \sin\frac{\psi}{2} \sin^2\frac{\psi}{4} + 1 \qquad (2\text{-}45)$$

Thus N varies linearly as a function of the radius of curvature. The total radiated power was shown to vary inversely as the square of the radius of curvature.

$$P_r = \frac{|E_i|^2 D^2 \nu_o^2}{32\pi k_o \eta_o r^2}\left[|Y|^2 K_1(\psi,\nu_o) + (Y + Y^*)K_2(\psi,\nu_o) + K_3(\psi,\nu_o)\right] \qquad (2\text{-}46)$$

where $K_1(\psi,\nu_o)$, $K_2(\psi,\nu_o)$ and $K_3(\psi,\nu_o)$ are given by

$$K_1 = \frac{\sin 2\psi}{3(\nu_o^2-1)(\nu_o^2-\cos^2\psi)}\left[\frac{3\nu_o^2+\cos^2\psi}{(\nu_o^2-\cos^2\psi)^2}+\frac{5\nu_o^2}{(\nu_o^2-1)(\nu_o^2-\cos^2\psi)}+\frac{11\nu_o^2+4}{2(\nu_o^2-1)^2}\right]$$

$$+\frac{\nu_o(2\nu_o^2+3)}{(\nu_o^2-1)^3\sqrt{\nu_o^2-1}}\left(3\frac{\pi}{2}-\tan^{-1}\frac{\sqrt{\nu_o^2-1}\cot\psi}{\nu_o}\right)$$

$$K_2 = -\frac{2}{3}\left[\frac{(3\nu_o^2+\cos^2\psi)\cos\psi}{(\nu_o^2-\cos^2\psi)^3}+\frac{3\nu_o^2-1}{(\nu_o^2-1)^3}\right]$$

$$K_3 = \frac{\sin 2\psi}{3(\nu_o^2-\cos^2\psi)}\left[-\frac{3\nu_o^2+\cos^2\psi}{(\nu_o^2-\cos^2\psi)^2}+\frac{\nu_o^2}{(\nu_o^2-1)(\nu_o^2-\cos^2\psi)}+\frac{\nu_o^2+2}{2(\nu_o^2-1)^2}\right]$$

$$+\frac{\nu_o}{(\nu_o^2-1)^2\sqrt{\nu_o^2-1}}\left(3\frac{\pi}{2}-\tan^{-1}\frac{\sqrt{\nu_o^2-1}\cot\psi}{\nu_o}\right)$$

where Y^* is the complex conjugate of Y.

CHAPTER III

EXPERIMENTAL SET UP AND MEASUREMENT PROCEDURE

The microwave model of the dielectric slab waveguide consisted of a strip of dielectric foam 9.2 cm in width, and about .95 cm in thickness. The dielectric foam was placed between two planar conducting sheets as shown in Fig. 6, thereby simulating a slab waveguide 2.7 wavelengths thick and of unbounded width. The two parallel conducting sheets on either side of the slab simulate unbounded width. These parallel plates are 360 cm in length and 240 cm in width each. The lower plate was held fixed and flat on a large table. The top plate was suspended from the ceiling and could be moved up and down using a pulley system.

As depicted in Fig. 7, each plate originally was a thin flat sheet of aluminum .2 cm in thickness and 360 × 120 cm width. In the laboratory it was important to use some kind of stiffening (thick channels of aluminum around its sides and plywood in the center of the plate for the top sheet to minimize the curvature caused by its weight). By making the top sheet movable it was very easy to change the shape of the slab inside these two plates like making bends with different radii or putting two parallel slabs with different dimensions next to each other and vary the separation in between, etc.

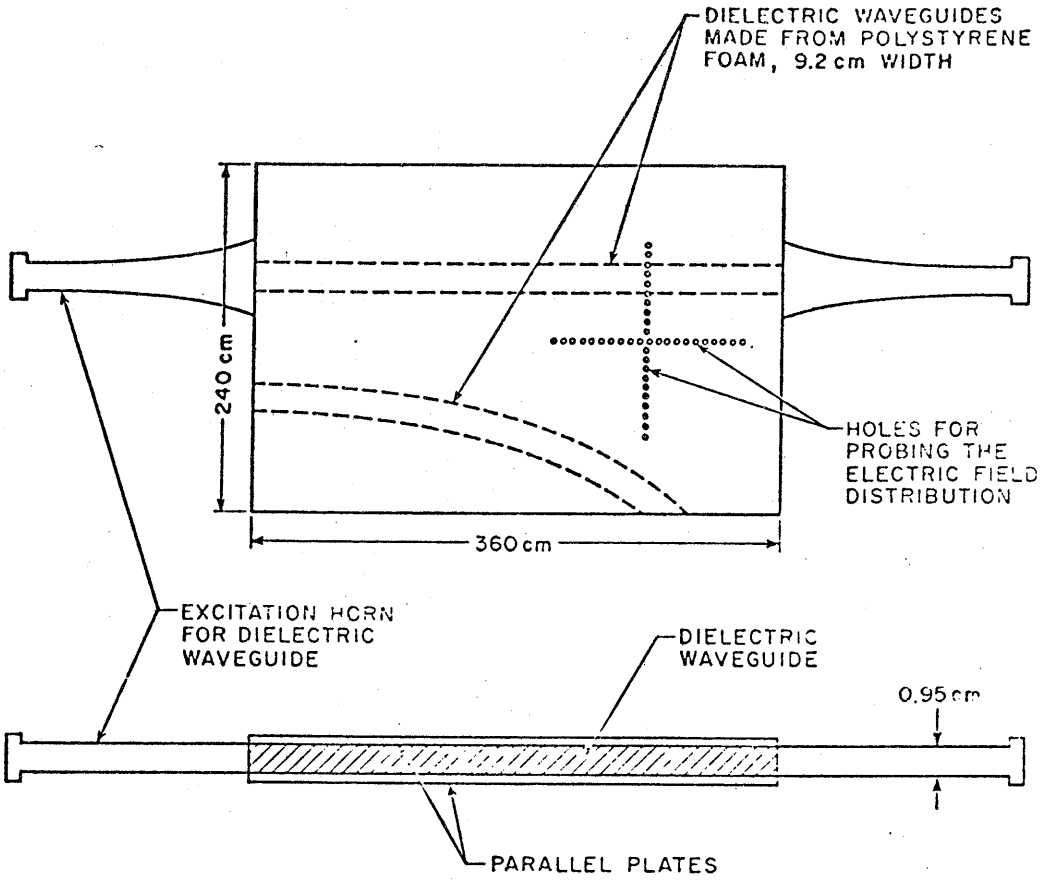

Fig. 6 Top and side view of the parallel plates.

To measure the transverse component of the electric fields, it was necessary to drill small holes .6 cm apart for insertion of the probe through the top sheet.

The model was excited by 9.0 GHz signal fed into a rectangular horn which flares from a standard x-band waveguide to a 25.4 cm by .95 cm multimode rectangular waveguide with a variable width profile over a length of one meter. The horn was then used to provide excitation at one end of the dielectric slab which, as was mentioned before, was placed between the 240 cm $\times$ 360 cm metallic parallel plates with separation of .95 cm as indicated in Fig. 8.

The dielectric slab is made of extruded polyethylene foam which has a relative permittivity between 1.03 and 1.04, which can be calculated using a logarithmic mixing rule. It is expressible in terms of the relative volumes occupied by the polyethylene and trapped air. By compressing foam slabs of different initial volumes into slabs of the same volume, a different refractive index for each slab can be achieved [9,10], furthermore these results are predictable using the above mentioned logarithmic mixing rule. The use of foam material provides an additional advantage in fabrication, design parameters such as cross-sections, spacings, and curvatures of straight and curved slabs can be met with precision. Experimental studies, such as power coupling between two guides, scattering pattern of curved guides at the bends,

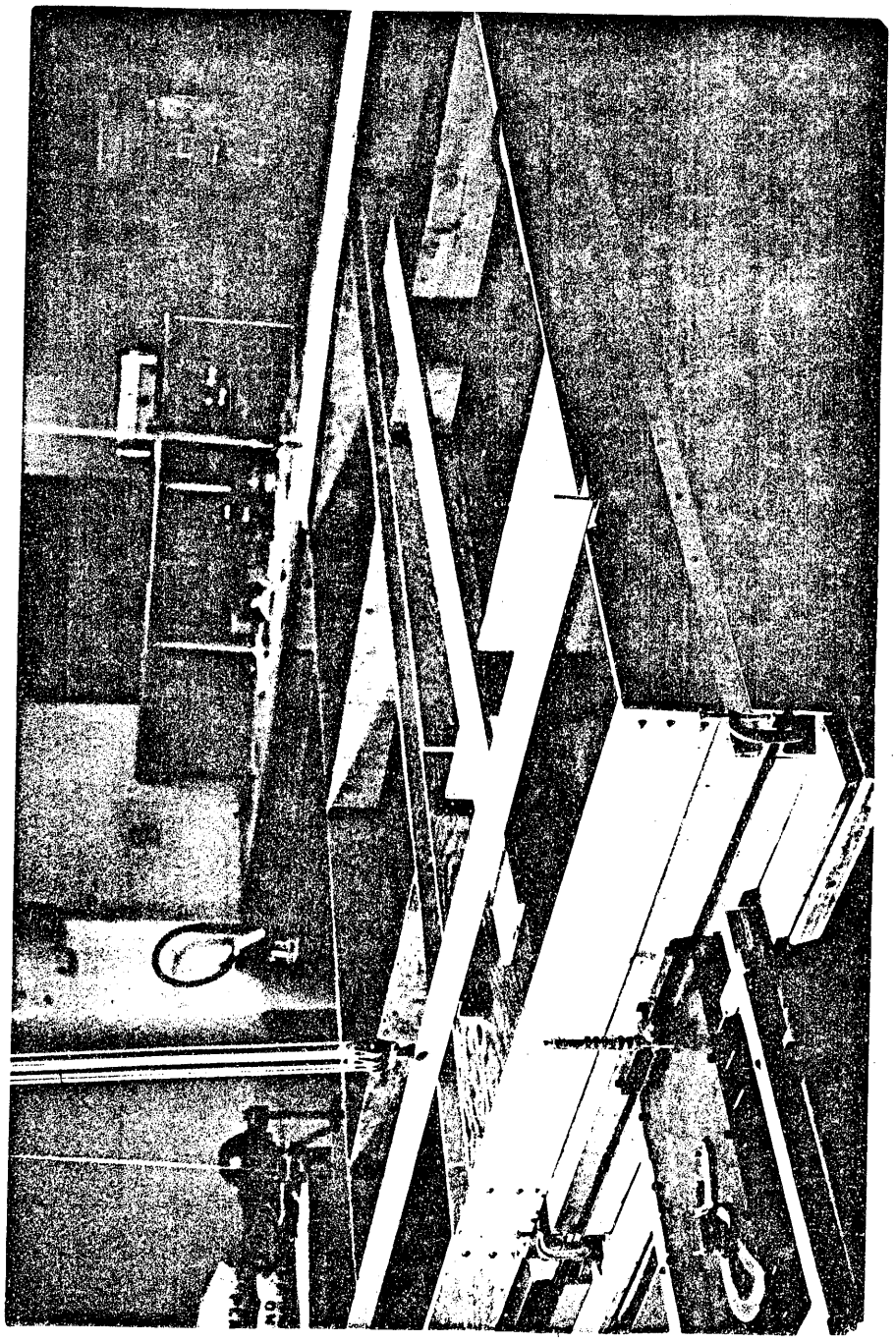

Fig. 8. Dielectric slab waveguide sandwiched between parallel plates .95 cm apart.

power loss due to continuous and scattering radiation in a curved section etc. conducted on the model give results that can be interpreted in terms of the actual optical waveguide.

In order to cut the foam to the shape required with reasonable accuracy, we have used either a high speed saw or a hot nicrome wire (5 Ω in resistance) carrying 1 amp of current.

For the design of a single mode dielectric slab waveguide, equation (2-11) can be used by assuming

$$pt = 0$$

Then

$$ht = k_o t \sqrt{n_1^2 - 1} \qquad (3\text{-}1)$$

The first odd mode has a cutoff frequency at $ht = \frac{\pi}{2}$, therefore to assume single mode operation the width of the slab should be chosen in such a way that the circle of equation (2-11) does not intersect the curve of equation (2-16), since the second mode comes at $ht = \frac{\pi}{2}$.

Choosing, $ht = 1.5$ will insure single mode operation. Hence equation (3-1) becomes

$$1.5 = k_o t \sqrt{n_1^2 - 1}$$

or

$$t = \frac{1.5}{k_o \sqrt{n_1^2 - 1}}$$

i.e. the width of slab, D, is given by

$$D = 2t = \frac{3}{k_o\sqrt{n_1^2 - 1}} \qquad (3\text{-}2)$$

where n_1 is the refractive index of the slab and $k_o = \omega_o\sqrt{\mu_o\varepsilon_o}$. With D given by equation (3-2), the TE_o mode is excited in the slab guide.

Measurements of the transverse field distribution were made with a miniature probe protruding through the holes on the top metal plate, therefore to take a complete set of measurements each hole has to be probed individually.

A serrodyne system [23] was used to measure the relative amplitude and phase of the electric field. Figure 9 shows a schematic diagram of the system. The Serrodyne system consists of an oscillator which feeds a signal of 9 GHz frequency into a travelling wave tube (TWT-Alfred 504). The output of TWT has a frequency of 9 GHz + 1000 Hz which is fed into the multimode rectangular waveguide horn that flares into the parallel plate and slab waveguide system. The output of the probe is fed into a crystal mixer along with the oscillator signal. The useful part of the output of the crystal is proportional to the product of the amplitudes of the two signals at their difference frequency (1000 Hz). It is this 1000 Hz signal which gives the informatin about the field being probed. Usually a signal 20 db below the output of TWT is coupled out and mixed with the oscillator signal to be used as a reference

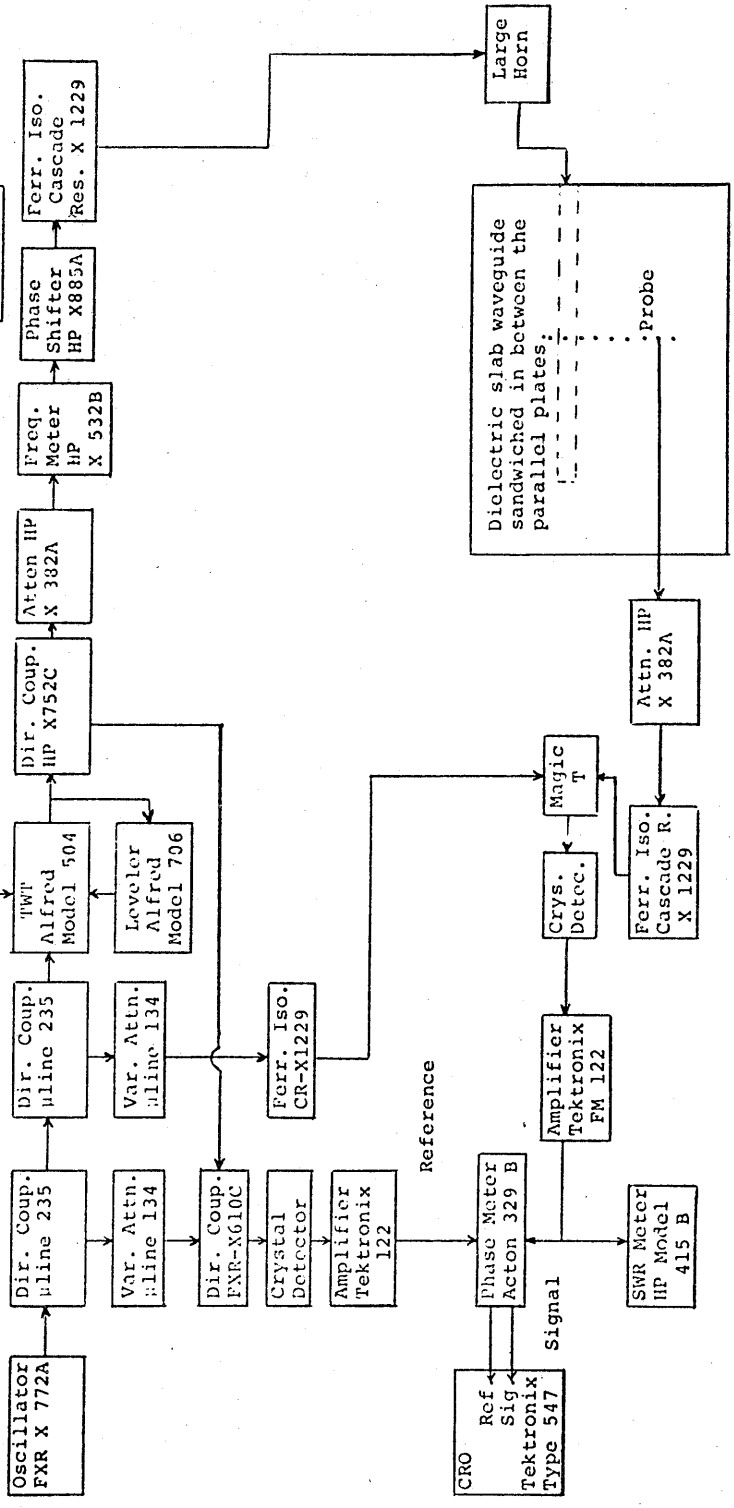

Fig. 9 The Measurement System

signal. The reference signal is held at constant amplitude. The standing wave meter, phase meter and scope respond only to the difference frequency of 1000 Hz in the crystal output. Hence the crystal output is amplified and used as the input to the standing wave meter, phase meter and scope.

The calibration for amplitude measurements needed in this experiment was given by Kerrigan [23]. A curve for the interpolation of a given set of calibrated amplitude data are shown in Fig. 10. Figure 10 interpolates logarithmically.

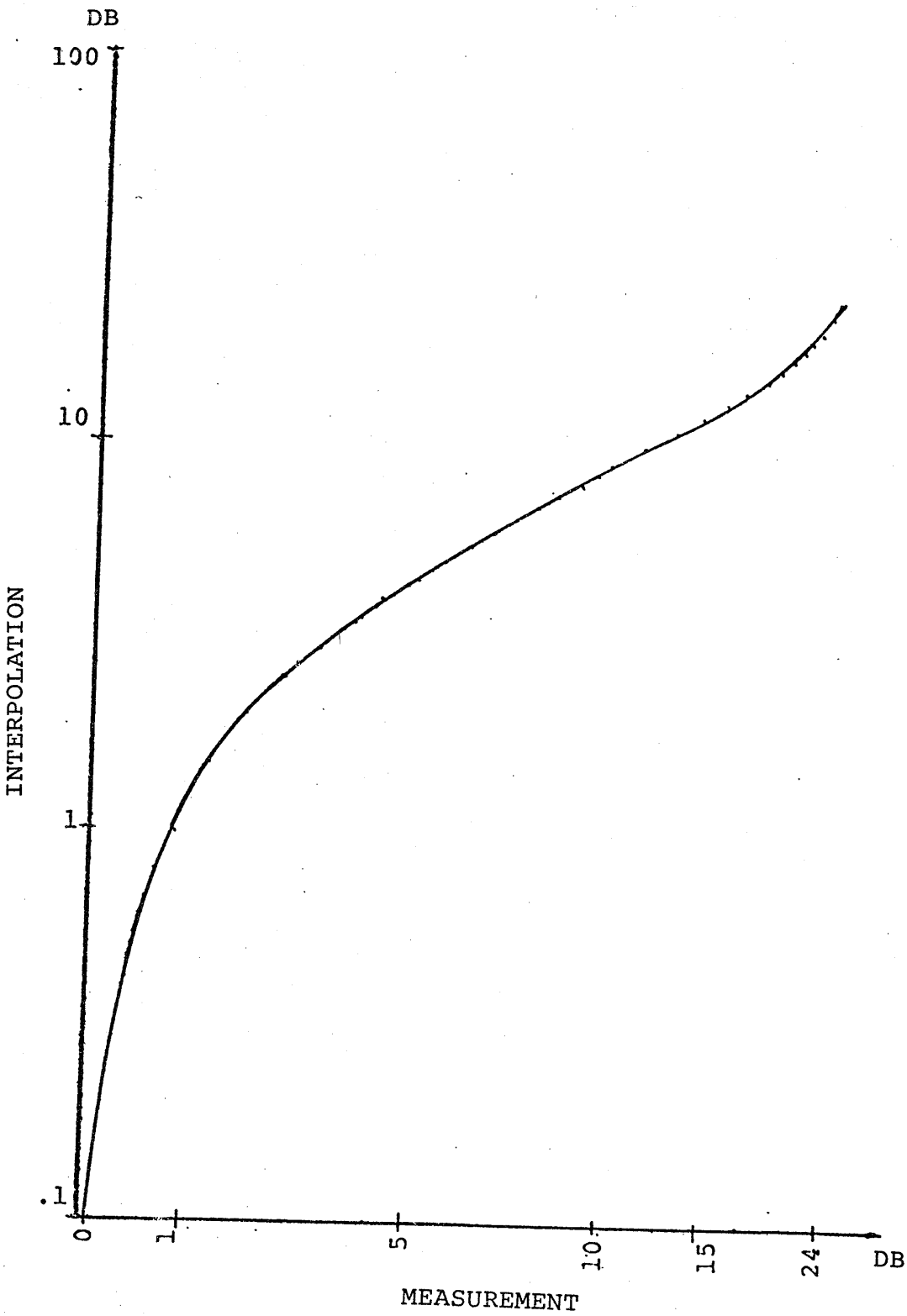

Fig. 10. LOGARITHMIC DATA INTERPOLATION CURVE

CHAPTER IV

SINGLE SLAB DIELECTRIC WAVEGUIDE

Following the design procedure given in Chapter III, Eq. (3-2) with $n_1^2 = \varepsilon_r = 1.03$ and an operating frequency = 9 GHz, the width of the slab can be calculated for single mode operation (TE_o mode) as

$$D = 9.2 \text{ cm} \quad \text{or} \quad 2.7\lambda$$

where $\lambda = 3.3$ cm is the free space wavelength.

Now using the experimental set up described in the previous chapter, the straight slab was placed in between the two parallel aluminum plates as shown in Fig. 8. At the end of the slab a matched termination was placed. This termination consisted of triangular tapered spears of a highly lossy carbon material that absorbs the radiated power from the end of the dielectric waveguide. The termination has little reflection due to the tapered design of it. The horn provides a reasonable source for the excitation of a surface mode.

Transverse field measurements were made at two different locations to determine whether the surface wave mode was successfully launched. As shown in Fig. 11, both the magnitude (calibrated) and phase of the transverse electric field

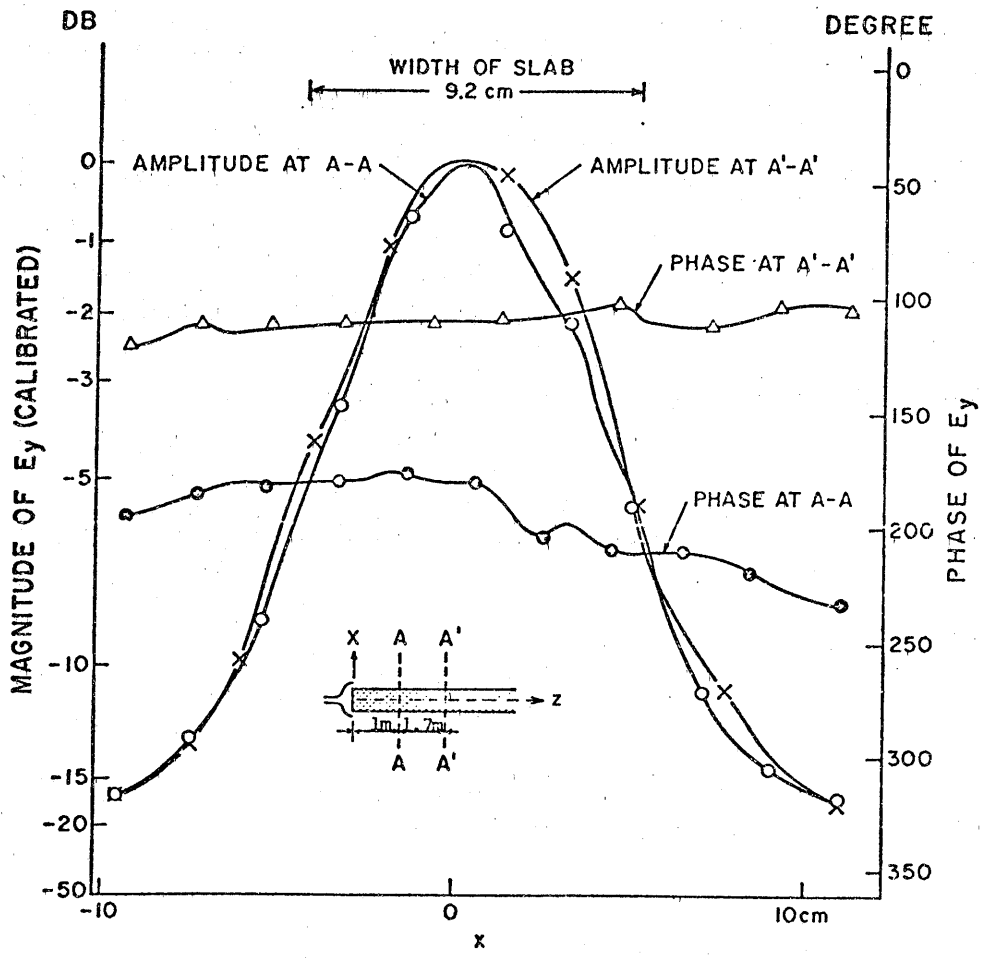

Fig. 11 Magnitude and Phase of the Transverse Electric Field Vs. Distance for 1 m (A-A plane) and 2.7 m (A'-A' plane) away from the horn.

were measured across the dielectric slab at distances of 1 meter (i.e. A-A plane) and 2.7 meter (i.e. A'-A' plane) away from the excitation horn. It was found that the spurious radiation from the horn has a strong influence on the shape of the field distribution at the A-A plane. At the A'-A' plane, however, there is little influence due to the spurious radiation.

A theoretical analysis has been made by solving the transcendental equations (2-10) and (2-11) for h and p, using numerical methods (see Appendix). Where h is the transverse propagation constant inside the dielectric slab (it is 20 m^{-1}) p is the transverse attenuation constant outside the slab (it is 26 m^{-1}). Equations (2-3) and (2-6) give the transverse field distribution inside and outside the dielectric waveguide respectively.

A theoretical and experimental plot of the magnitude (on a linear db scale) and phase of the transverse electric field are shown in Fig. 12. There is very good agreement between the two curves.

Electromagnetic field measurements for Figs. 11 and 12 were made at two different times. Different scale systems were used in plotting the magnitudes for the two figures. These measurements were made for the same slab width (9.2 cm) at a distance of 2.7 m from the horn (A'-A' plane). More data points were taken in plotting the experimental curve

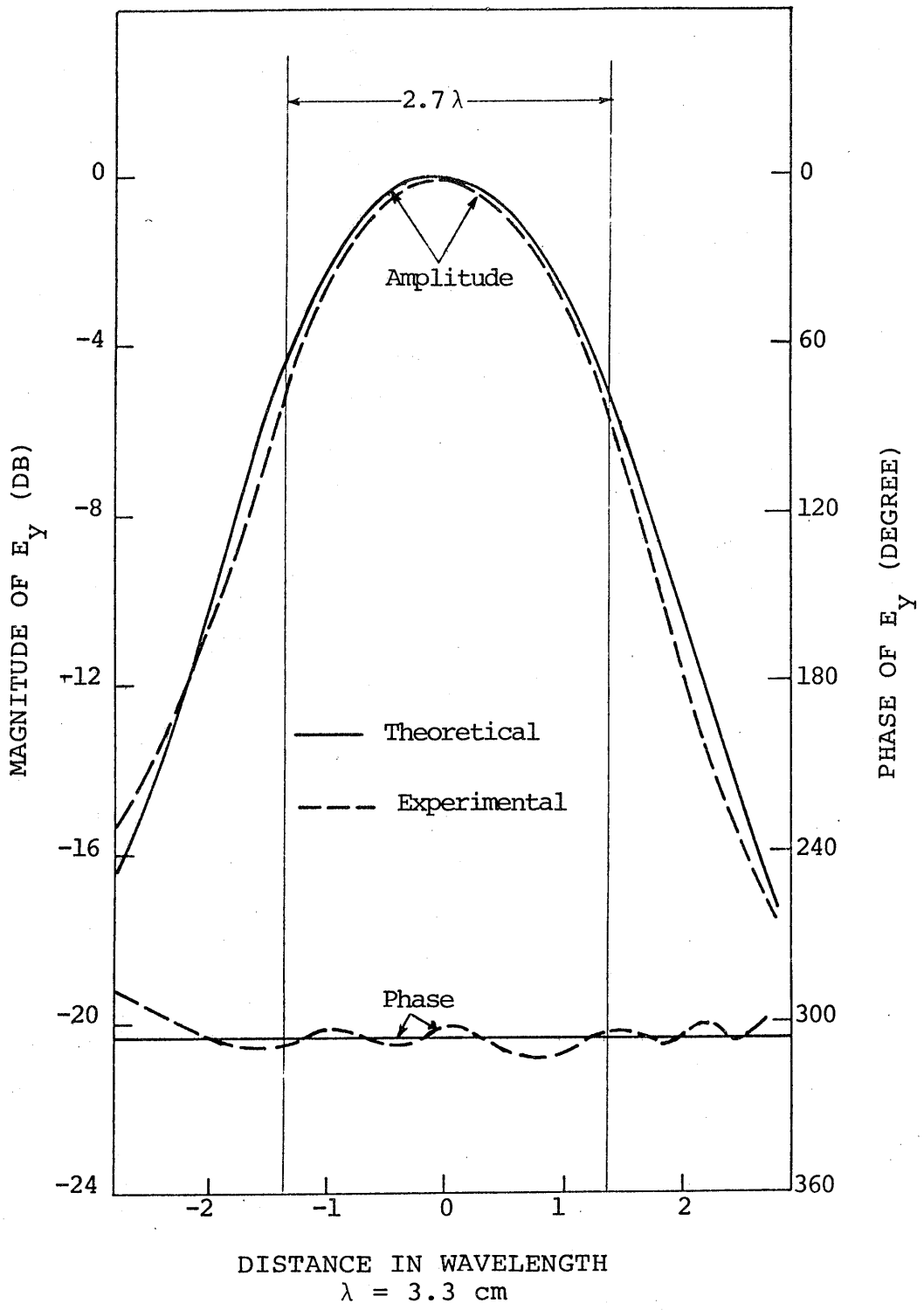

Fig. 12. Magnitude and Phase of the Transverse Electric Field Vs. Distance for a Single Slab Waveguide

in Fig. 12. Therefore some slight difference in phase can be seen in comparing the phase of Fig. 11 (at A'-A' plane) and that in Fig. 12 (experiment).

CHAPTER V

COUPLING BETWEEN TWO DIELECTRIC SLAB WAVEGUIDES

In this chapter we are concerned with the experimental investigation of the coupling between two dielectric slab waveguides, but experimental results will be compared with theory.

In the manner described in Chapter IV, a surface-wave mode was launched in a single dielectric slab. The addition of another similar slab parallel to the first (excited waveguide) as shown in Fig. 13 will permit coupling some power from the first slab to the second. This is due to the fact that the field of a surface-wave mode extend indenfinitely into the region outside the waveguide. Since there is a continuous flow of power between the first slab and the second, the field in the second waveguide will be enhanced until a certain distance L is reached. At this point there is a complete power transfer from the first waveguide to the second. This complete power transfer happens just in the degenerate (both waveguides having the same phase velocity) case. For the non-degenerate situation

a partial power transfer will occur. This process continues indefinitely with power being transferred back and forth between the two waveguides. At the operating frequency 9 GHz, it was difficult to experimentally verify the theory by finding the distance over which there is a complete power transfer since the coupling distance is very large (in the range of 10 meters for the degenerate case with a separation of 1.5λ). This means at least a 10 meter length of parallel metal plates would be needed.

Experimentally, we investigated the case where the horn provides the only excitation source for the slab. This kind of excitation has some disadvantages in the case of coupling because of the radiation that flares sideways as shown in Fig. 13 and causes some changes in the amplitude and phase of the second waveguide.

Practically, it is not possible to have a unit magnitude of electric field at the first waveguide and exactly zero amplitude at the second, as we have assumed in the theoretical analysis of coupling in Chapter II. However as will be detailed in the following, we had good agreement between the theoretical and experimental curves of the electric field

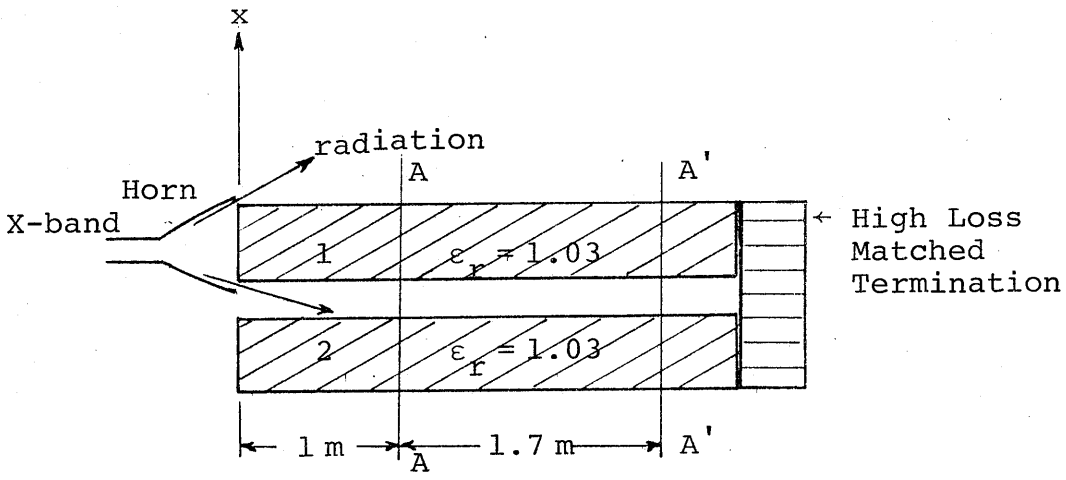

Fig. 13: Two Parallel Slab Waveguides.
Slab 1 is excited by a horn.

magnitudes in the second waveguide beyond certain distance. This distance is greater for the degenerate case.

Our purpose was to study the coupling characteristics as a function of separation for both degenerate and non-degenerate type modes.

(a) Two parallel and similar slabs (degenerate case):

Transverse electric field measurement was done, as for the single slab case, at two different places 30 wavelenth (A-A plane) and 81 wavelength (A'-A' plane) away from the horn. Figures 14, 15 and 16 show the magnitude and the phase of the transverse electric field Ey in the two waveguides at the two planes (A-A) and(A'-A'). It is evident

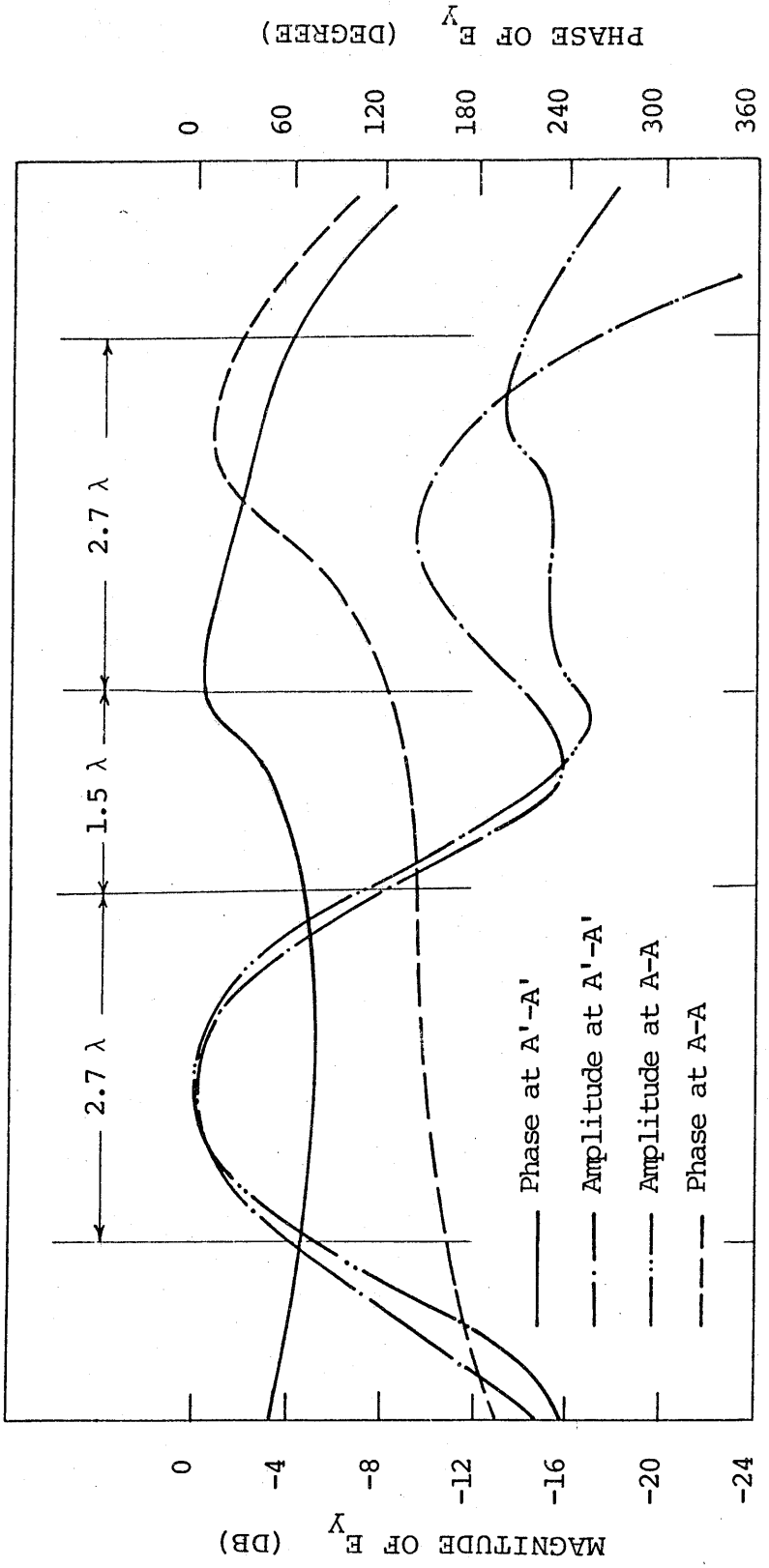

Fig. 14. Magnitude and Phase of the Transverse Electric Field Vs. Distance for 1 m (A-A plane) and 2.7 m (A'-A' plane) away from the horn for two parallel and similar waveguides with a separation of 1.5 λ. The left waveguide is excited by the horn.

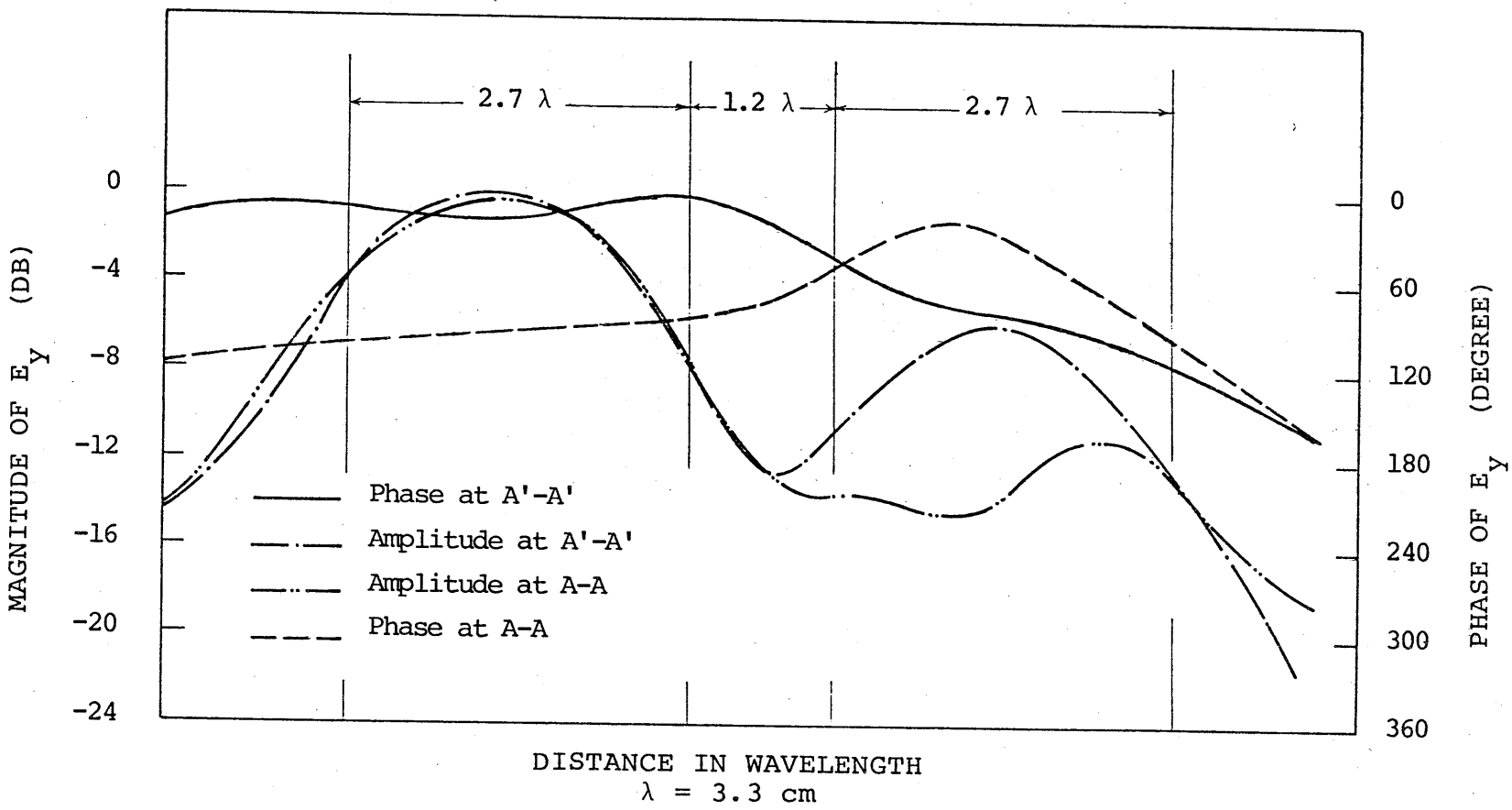

Fig. 15. Magnitude and Phase of the Transverse Electric Field Vs. Distance for 1 m (A-A plane) and 2.7 m (A'-A' plane) away from the horn for two parallel and similar waveguides with a separation of 1.2 λ. The left waveguide is excited by the horn.

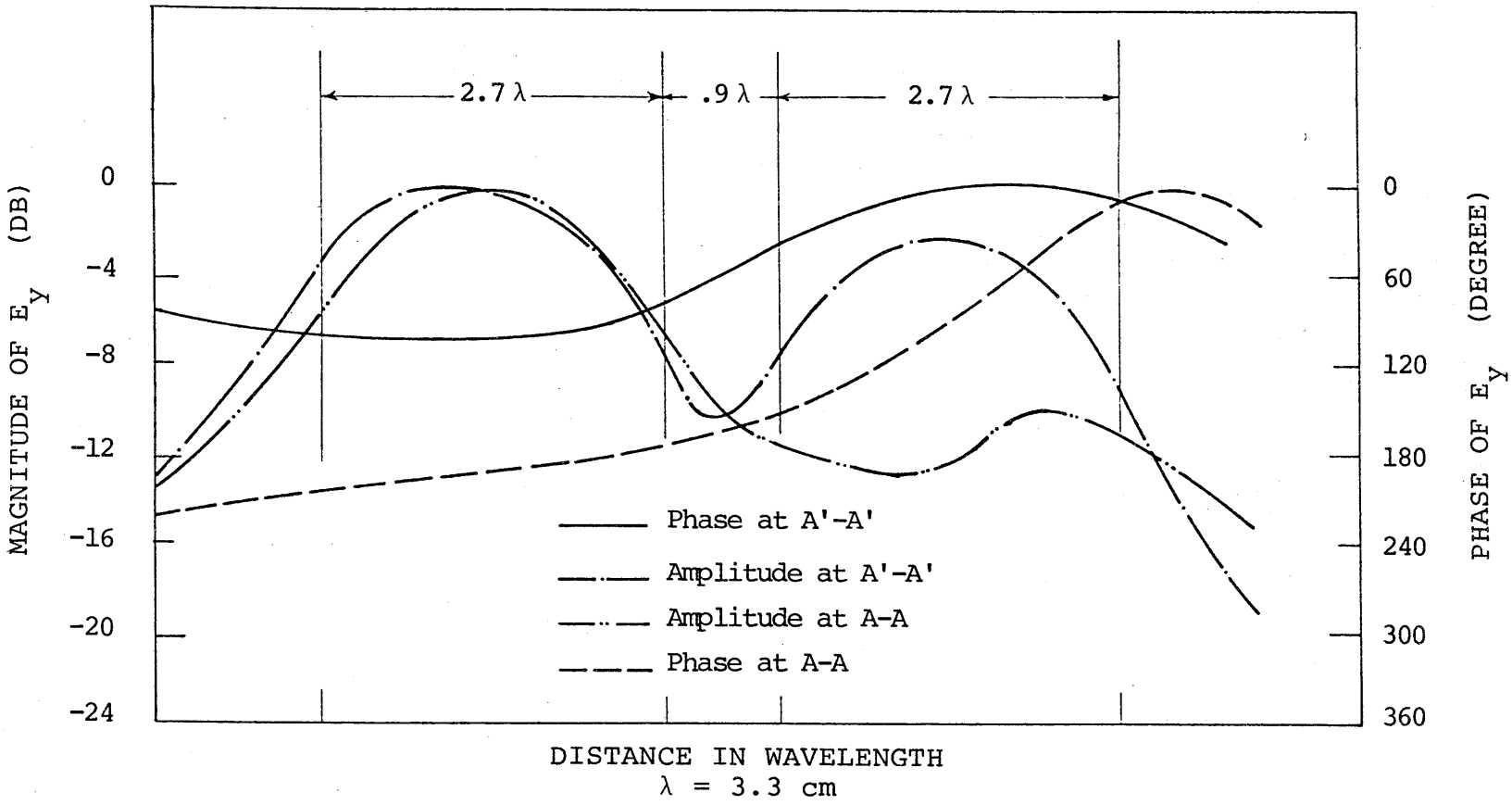

Fig. 16. Magnitude and Phase of the Transverse Electric Field Vs. Distance for 1 m (A-A plane) and 2.7 m (A'-A' plane) away from the horn for two parallel and similar waveguides with a separation of .9 λ. The left waveguide is excited by the horn.

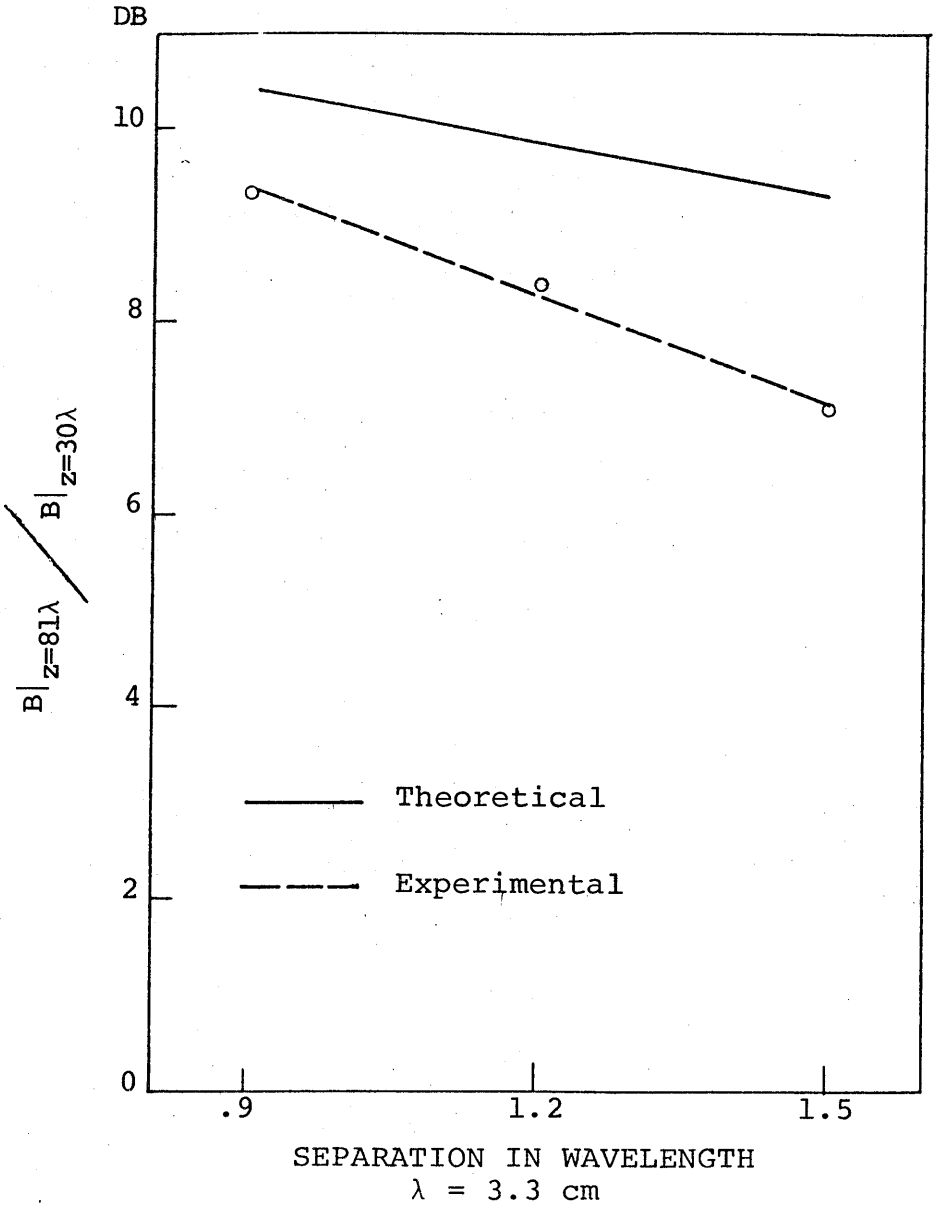

Fig. 17. The Relative Increase in the Max Amplitude of the Electric Field in the Second Waveguide from the A-A Plane to A'-A' Plane for the Degenerate Case.

from the phase characteristics at the A-A plane, that the radiation coming out of the horn has a strong influence on the field of the second waveguide. Also there is no clear surface type mode at the second slab at this distance because the coupling length is very large (approximately 9.6, 7.4 and 5.7 meters for the three different types of separations 1.5λ, 1.2λ and $.9\lambda$ respectively), while our measurement is at 1 meter from the horn. The strong influence of radiation at this plane will make it difficult to obtain good agreement with the theoretical analysis. At the A'-A' plane, the surface wave type mode has the shape predicted by theory. Thus the unwanted radiation from the horn has little influence on the amplitude but it does have some influence on the phase. It is interesting to note that as the slab separation becomes smaller the magnitude of the electric field in the second slab-increases. This indicates that the coupling distance L (for complete power transfer) decreases as the separation gets smaller.

Theoretically, Kuester and Chang [8] solved for the field in the waveguides, assuming that each mode is normalized to unit power carried in the z-direction

$$\bar{E}^{+} = A_1(z)\ \bar{E}_1^{+} + A_2(z)\ \bar{E}_2^{+} \tag{5-1}$$

where

$$A_1(z) = \cos(\Delta\beta z)\ e^{-i\beta z} \tag{5-2}$$

$$A_2(z) = -i\ \sin(\Delta\beta z)\ e^{-i\beta z} \tag{5-3}$$

and β is the propagation constant along the z axis for a single slab waveguide. $\bar{E}_1^+$ and $\bar{E}_2^+$ are the single slab transverse field distribution which are equal for similar waveguides.

By letting

$$B = \left| \frac{A_{2\ max.}}{A_{1\ max.}} \right|$$

We have plotted the experimental and theoretical curves $B|_{z=81\lambda}/B|_{z=30\lambda}$ in Fig. 17. Also Table I represents the differences between the two curves in terms of percentage of error.

Table I

Separation	Relative Error	Theoretical Coupling Length In Meters
.9 λ	12%	5.7
1.2 λ	16%	7.4
1.5 λ	23%	9.6

It would seem that error in this case is primarily due to

(1) The coupling length is very large while after one meter distance (A-A plane) measurement is hard to detect a clear shape of a surface wave mode in the second waveguide. It is interesting to note from Table I that as the coupling length increases the relative error between the theory and experiment

increases also. Although a good result were measured at the plane A'-A' (2.7 m away from the horn) there is still another problem, radiation from the horn that contributed to the error.

(2) The radiation that flares from the horn was mentioned earlier as having a strong influence (causes the enhancement of the electric field) at the plane A-A. Therefore a comparison in the relative amplitude at the two different planes will be less than anticipated from the theory.

From equations (5-2) and (5-3), the phase of Ey across each slab should be 90°. Experimentally, if we look at the difference in the average variation of phases in the two slab waveguides, it will be approximately 100°. This is in a good agreement with the theoretical analysis. The phase in the first waveguide behaves like a constant, which is the theoretically predicted value while the phase in the second slab has a wide variation. This could be the effect of radiation coming out of the horn.

(b) Two parallel but different width slab waveguides (Non-degenerate case):

This discussion is similar to that for the degenerate case except for some minor points. The first slab was kept at the same width 2.7λ as previously while the second slab

was designed so that the wave would propagate little faster than the wave in the first waveguide if it were isolated from the first slab. A .4% increase in wavelength in the second waveguide with respect to the first will result in

$$\lambda_2 = 1.004\lambda_1$$

$$\beta_2 = \frac{250}{251}\beta_1$$

$$\varepsilon_r k_o^2 - \beta_2^2 = h_2^2$$

Since β_1 is known for a single slab with width $D = 2.7\lambda$, it is easy to find h_2^2 and p_2^2 given by

$$p_2^2 = (\varepsilon_r - 1)k_o^2 - h_2^2$$

Hence using $\frac{p_2}{h_2} = \tan h_2 t_2$ we can solve for t_2.

Thus $D_2 = 2t_2 = 5.2$ cm

or $D_2 = 1.6\lambda$, where $\lambda = 3.3$ cm is the free space wavelength.

t_2 is the half width of the second slab.

h_2 is the inside slab transverse propagation constant.

p_2 is outside the slab transverse decay constant.

After placing the smaller slab parallel to the first, measurements of the transverse field distribution were made in the manner described in part (a) of this chapter. Figures 18, 19 and 20 show Ey as a function of distance for 3 different separations 1.5λ, 1.2λ and $.9\lambda$. It is noted that the

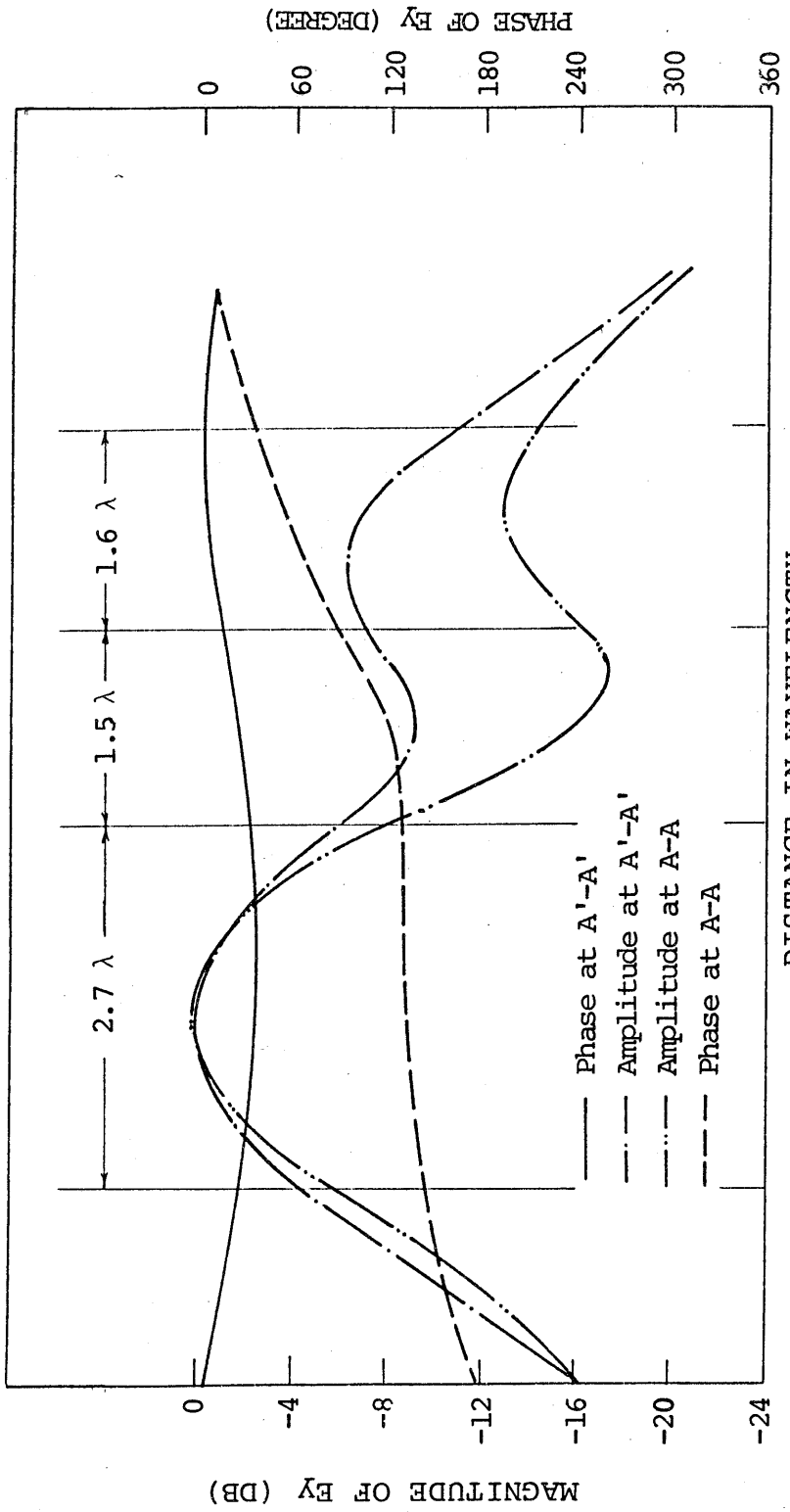

Fig. 18. Magnitude and Phase of the Transverse Electric Field Vs. Distance for 1 m (A-A plane) and 2.7 m (A'-A' plane) away from the horn for two parallel waveguides of different widths with a separation of 1-5λ. The left waveguide is excited by the horn.

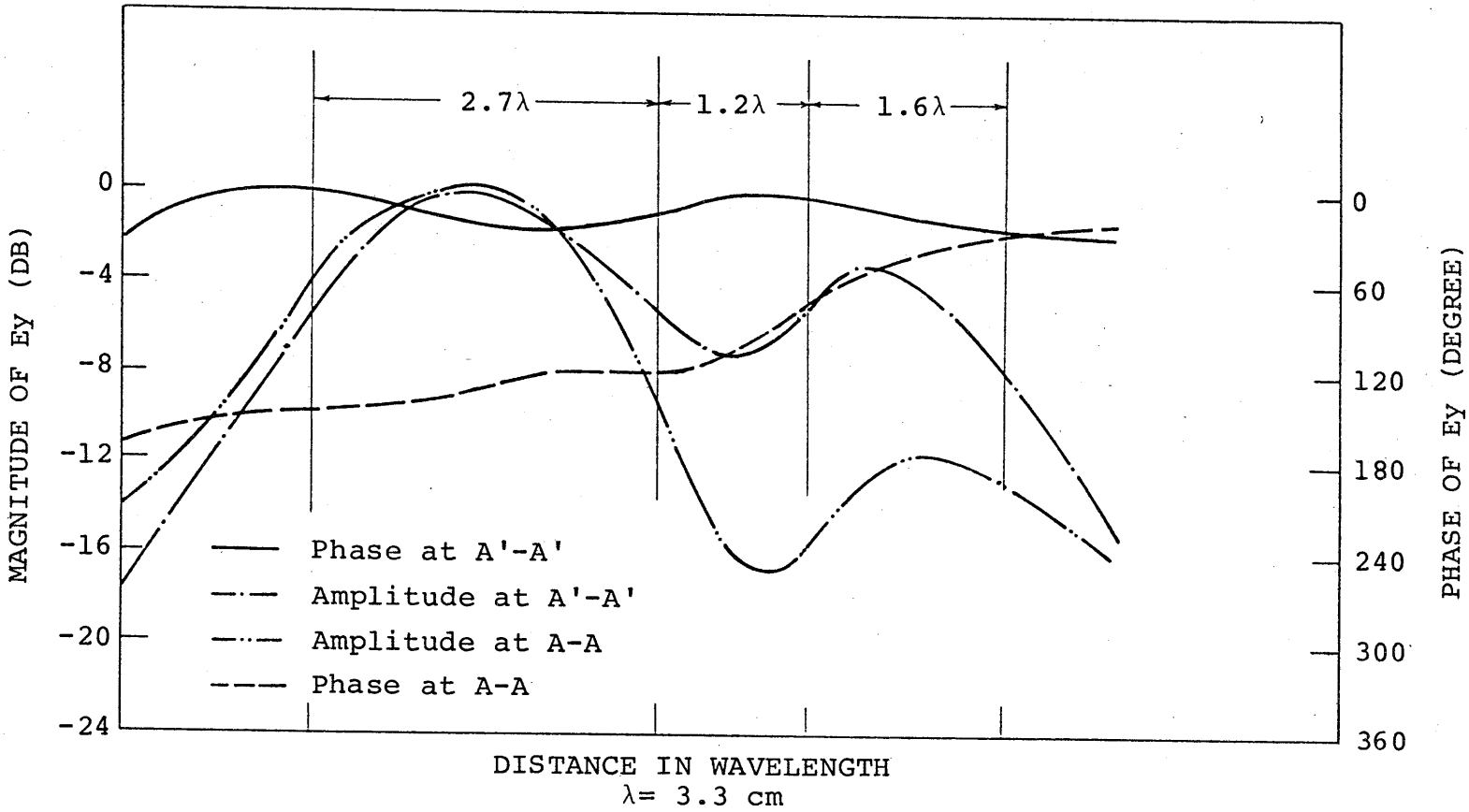

Fig. 19. Magnitude and Phase of the Transverse Electric Field vs. Distance for 1 m (A-A plane) and 2.7 m (A'-A' plane) away from the horn for two parallel waveguides of different widths with a separation of 1.2λ. The left waveguide is excited by the horn.

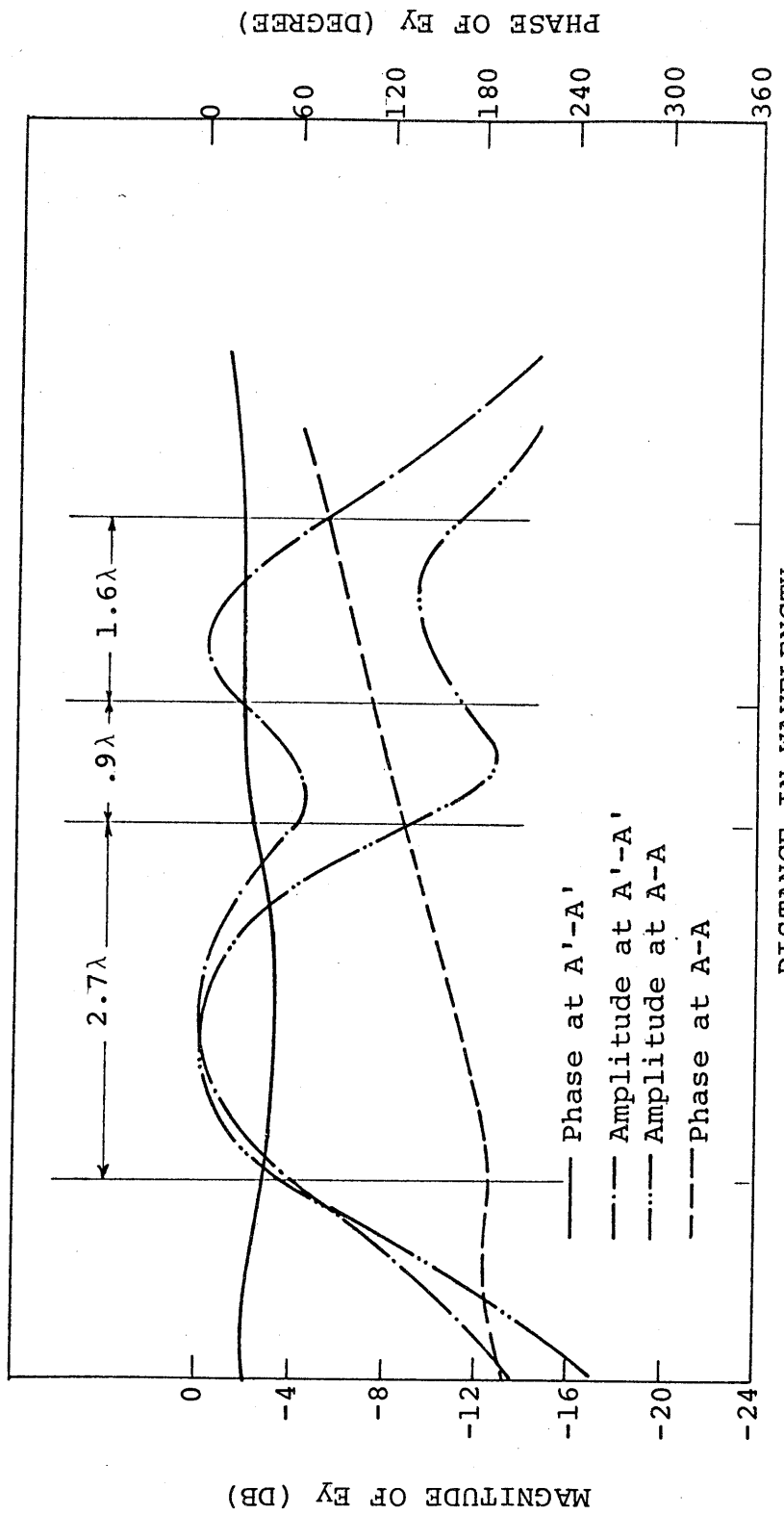

Fig. 20. Magnitude and Phase of the Transverse Electric Field vs. Distance for 1 m (A-A plane) and 2.7 m (A'-A' plane) away from the horn for two parallel waveguides of different widths with a separation of .9λ. The left waveguide is excited by the horn.

amplitude in the smaller waveguide, for fixed separation compared with the amplitude for the degenerate case at the same distance from the horn 81 (A'-A' plane) has increased. This is due to the decrease in the coupling length for the non-degenerate case.

As mentioned in part (a) of this chapter, it is required that the power in each waveguide be normalized to a unit magnitude in each waveguide. Therefore using

$$P = 1 = \frac{\beta}{\omega\mu_o}\int_o^\infty |Ey|^2 dx$$

the ratio between the two amplitudes in the two slabs is

$$\frac{A_{e2}}{A_{e1}} = \left(\frac{\beta_1 t_1 + \beta_1/p_1}{\beta_2 t_2 + \beta_2/p_2}\right)^{\frac{1}{2}}$$

Using equation (2-30) and the above normalization factor, we can plot the relative amplitude of Ey in the second waveguide as a function of separation at two different distances, as shown in Fig. 21. As in the degenerate case the quantity plotted is $B|_{z=81\lambda}/B|_{z=30\lambda}$. The two theoretical and experimental curves match up very well with error percentages as shown in table II.

TABLE II

Separation	Relative Error	Theoretical Coupling Length in meters
.9λ	7%	3.1
1.2λ	1%	3.5
1.5λ	11%	3.8

The reason for the relatively good comparison in this case is that the coupling length is shorter now and more within the range of our experimental equipment. The surface wave type mode in the second waveguide as shown in Figs. 18, 19 and 20, well shaped at the plane A-A (1 meter from the horn) while in the degenerate case it was not.

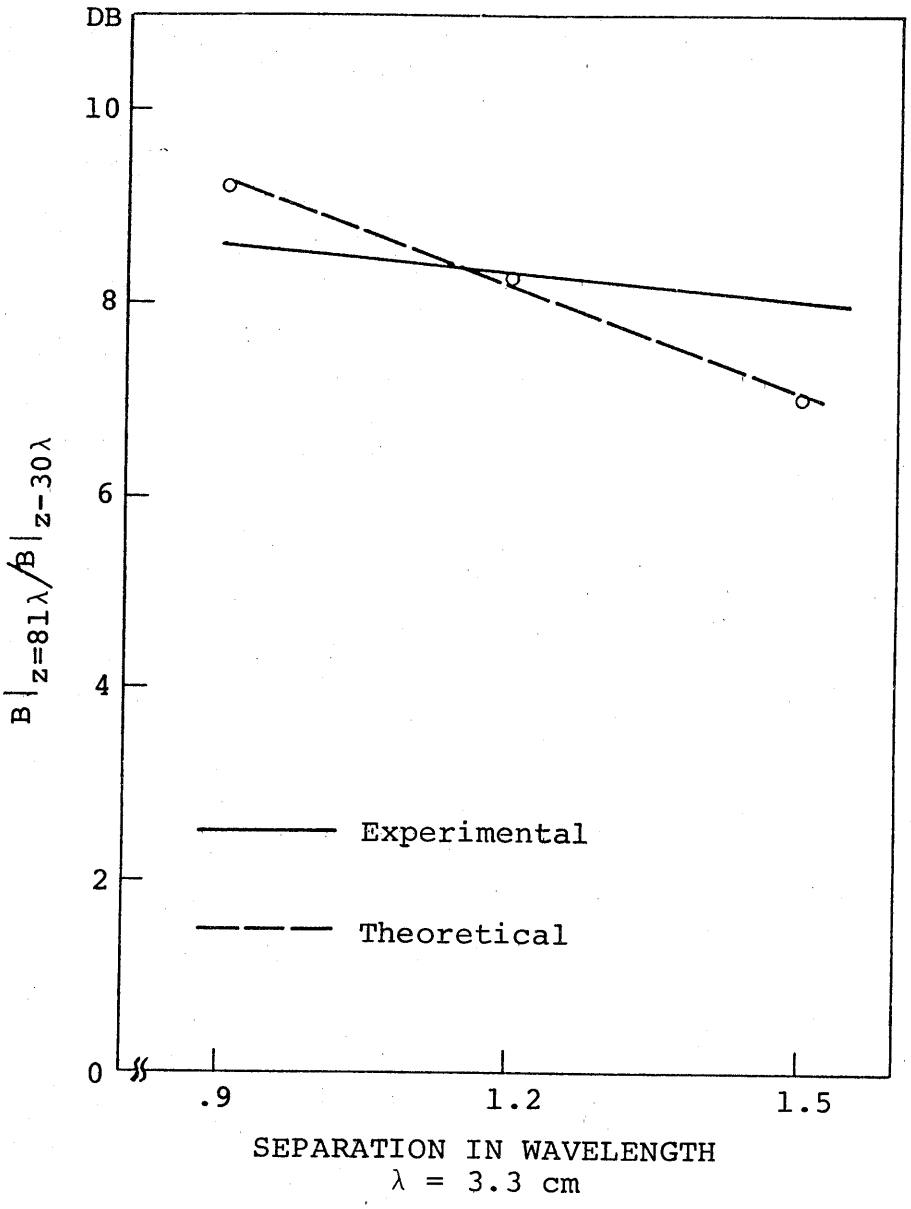

Fig. 21. The Relative Increase in the Max. Amplitude of the Electric Field in the Second Waveguide from the A-A Plane to A'-A' Plane for the Non-degenerate Case.

CHAPTER VI

RADIATION FROM BENDS IN DIELECTRIC SLAB WAVEGUIDE

In this chapter several aspects of the radiation from bends was investigated experimentally. The investigation included

(a) Effects of the transition from straight to curved dielectric slab.

(b) Propagation within a circular bend between two discontinuities.

(c) Minimization of radiation from bends.

(d) Far field radiation pattern measurements.

Radiation from a circular bend without transitions has been analyzed by Marcatili [15], Lewin [17] and Chang and Barnes [11]. These studies were limited to just finding the radiated power from a circular section only. S. Maley [12], later on, analyzed the far field pattern of a circular bend joining two discontinuities. These investigations are mainly theoretical in nature while there are few experimental studies. Neuman [18] made measurements on waveguides with electric fields having constant magnitude and constant phase angle and with a geometric configuration consisting of a straight section connected to a circular bend.

Using the same experimental model as described in Chapter III, the following experiments were performed.

(a) Propagation through a transition from straight to curved dielectric slab waveguide:

Here, the concern is with the launching of a single surface wave mode into a straight section (about 1.5m long) which is connected to a curved slab, having a radius of curvature equal to 3.5 meters. A high loss, triangular tapered type termination was placed at the end of this section as a matched termination. Magnitude and phase measurement of the transverse electric field along the radial direction on the curved structure (i.e. A'-A' plane) were made. As shown in Fig. 22 the angle of measurement with respect to the straight section is about 30°. Also included is the transverse field distribution along the straight section at a distance of 1 meter from the horn (i.e. A-A plane), in order to check the excitation of single surface wave mode.

As it can be seen the field distribution pattern (at the A'-A' plane) and therefore the power carried by the principle mode inside the slab, appear to have shifted towards the outer slab surface. Outside the slab in the exterior region, the field has an oscillating character. This is due to the interference between the continuous radiation along the curved section and the scattered field from the end of

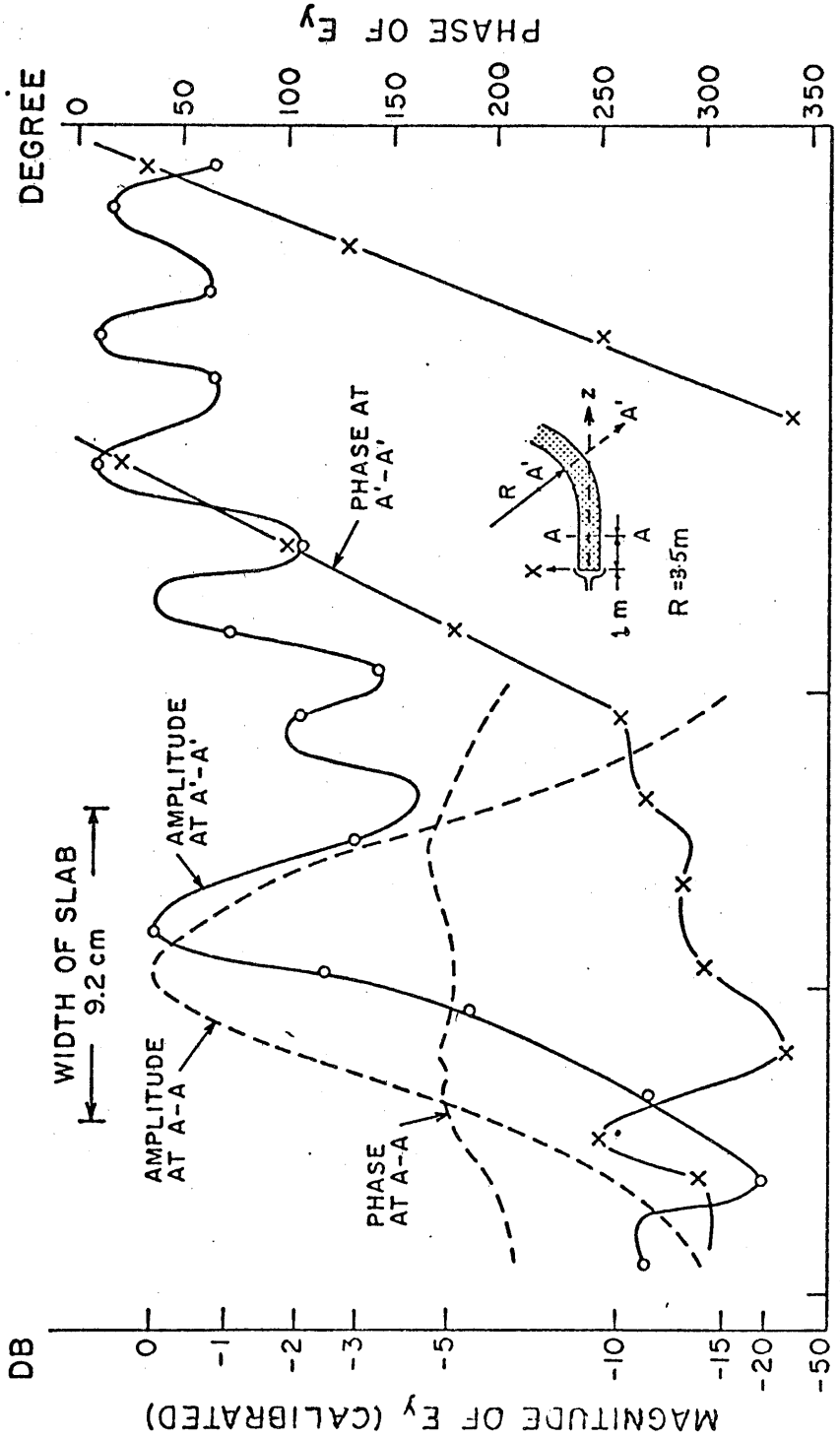

Fig. 22 Magnitude and Phase of the transverse electric field vs. distance on a curved and straight section.

the straight section. The continuous radiation can be explained from the viewpoint of the shift in the phase velocity along the slab direction. The separation between two constant phase fronts $\theta = \theta_1$ and $\theta = \theta_2$ increases continuously as a function of radial distance. Therefore for those waves farther from the slab surface, they have to travel faster in order to maintain a planar uniform phase front with those closer to the slab. As was mentioned in Chapter II, at a radial distance equal to that of the turning point, $\rho_o = \nu_o R$, the phase velocity $\rho\frac{d\theta}{dt}$ is exactly the speed of light. Beyond this point, wave has to travel faster than the speed of light and hence, is forced to radiate in the radial direction. Since a curved section can be thought of as an inhomogenous straight waveguide any wave incident from the straight waveguide (homogenous) on the curved part (inhomogenous straight slab), will have some scattering effect. Hence the direct scattering (caused by the discontinuity) is as important as the continuous radiation from just the curved section in determining the near-zone field distribution in the outer slab boundary.

(b) Circular bend between two discontinuities:

Similar to part (a) of this chapter, the transverse field distribution along the radial direction for a curved structure between two straight waveguides was measured. This part is

different from part (a) for the addition of a straight waveguide at the end of the curved section. Also a matched, high loss termination was placed at the end of the added straight section. These measurements were made for three different radii $R = 60\lambda$, 90λ and 120λ having angles of bend of 64°, 38° and 28° between the two straight sections respectively. As indicated in Figs. 23 and 24, the magnitude (on a linear db scale) and the phase of Ey along the radial direction (i.e. the phase A'-A') were plotted. It is interesting to note that the strength of the oscillating field on the exterior region of the slab increases as the radius of curvature gets smaller.

If we just consider the continuous radiation from the curved guide, it can be seen from eq. 2-37 that when R decreases α becomes larger and hence the field strength inside the slab decreases. We have plotted in Fig. 27 the maximum transverse electric field inside the curved structure, at certain angle θ from the straight section in region 1, with respect to the maximum electric field inside the straight waveguide. This gives an indication of the amount of power radiated by the bend. The radiated field due to just the continuous radiation can be calculated from equation 2-32. The following was plotted as (Theoretical-Chang)

$$20 \log_{10} \left| \frac{E_{c\ max.}}{E_{s\ max.}} \right| = - 20\alpha R\theta \log_{10} e = -8.6859\alpha$$

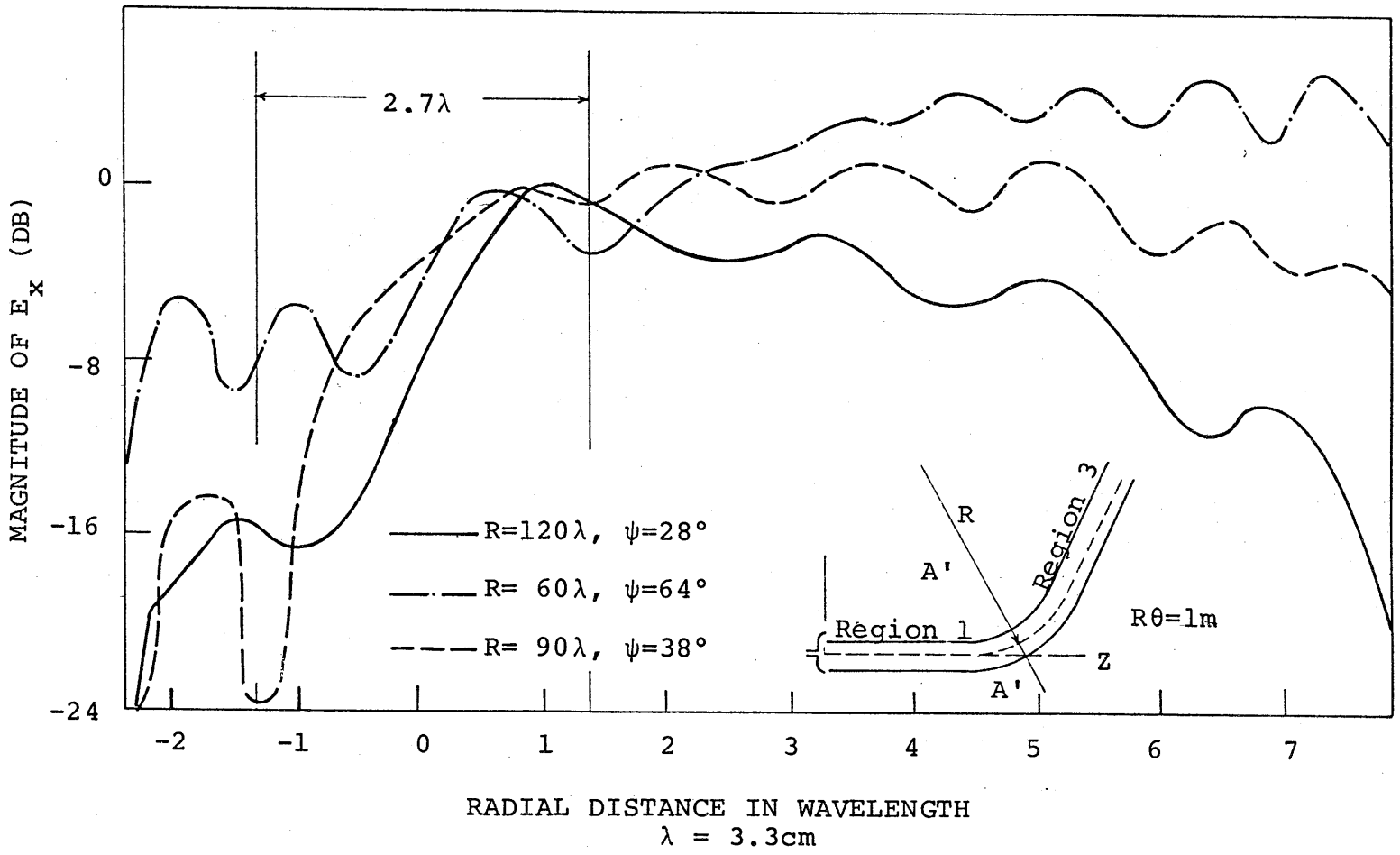

Fig. 23 Magnitude of the Transverse Electric Field Vs. Radial distance for three different radii. The position of A'-A' plane is at 1 meter away from the straight section in region 1.

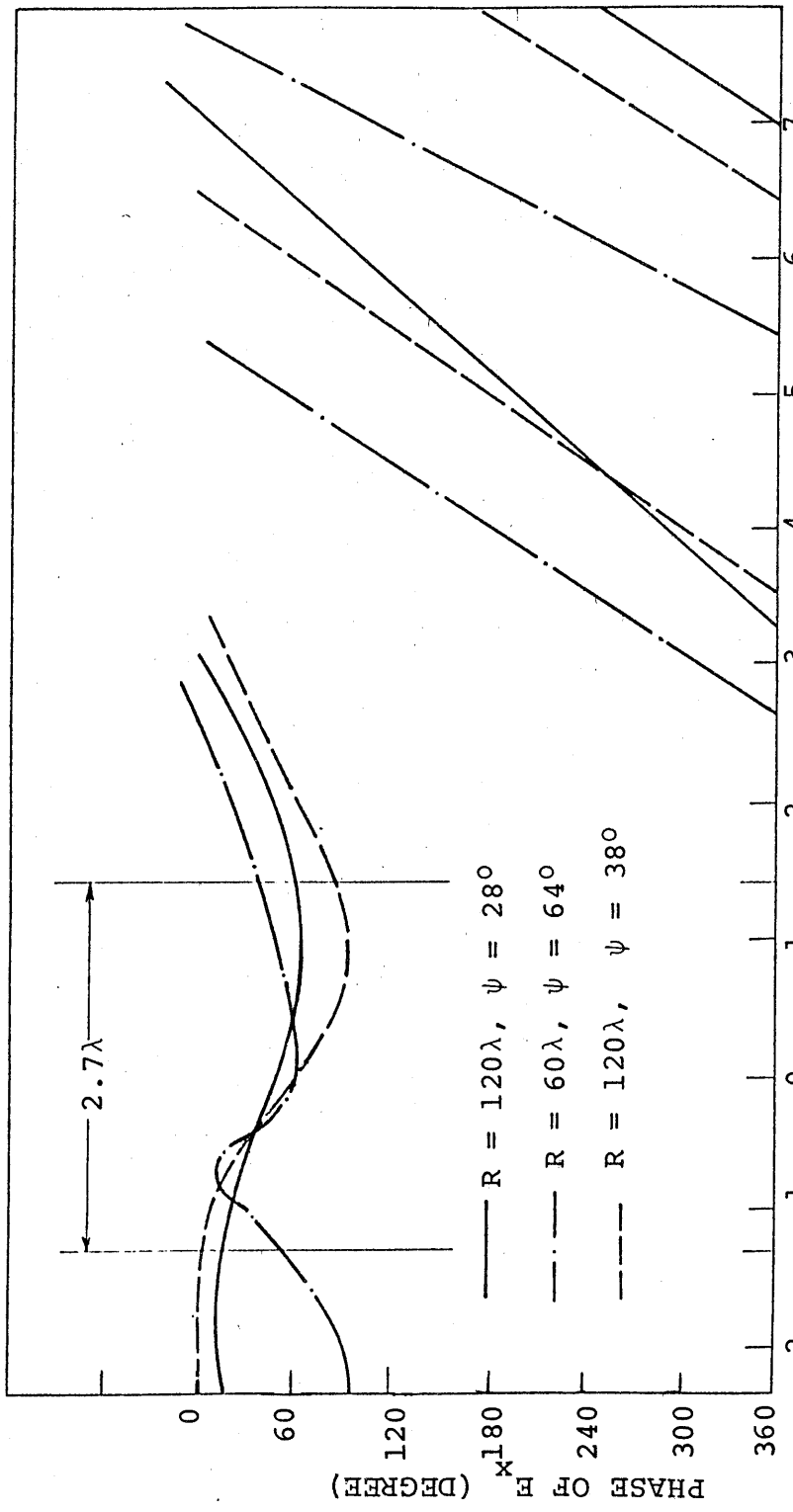

Fig. 24 Phase of the Transverse Electric Field shown in Fig. 23 Vs. Radial distance

where $R\theta$ = 1 meter for the three radii $R = 60\lambda$, 90λ, and 120λ and $E_{c\ max.}$ is the max. transverse field inside the curved guide.

$E_{s\ max.}$ is the max. transverse field inside the straight waveguide. There is a computer program in the Appendix to evaluate α which is the attenuation constant.

Included in Fig. 27 are the additional effects due to the discontinuity between the straight and curved waveguide sections. The theoretical analysis was taken from [12]. Equation 2-46 gives the total radiated power due just to the discontinuity. It turns out, for all cases where $R = 60\lambda$, 90λ and 120λ , that the radiated power can be given by

$$P_r = 2.63\ 10^{-4}\ \frac{|A_e|^2}{R^2}$$

and the input power P_i flowing in the z direction per unit length in the x direction in the straight waveguide is

$$P_i = \frac{1}{2}\int_{-\infty}^{\infty} \mathrm{Re}(\bar{E} \times \bar{H}^*)\,dx = \left(\frac{\beta t + \beta/p}{2\omega\mu_o}\right)|A_e|^2$$

or

$$P_i = 7.12\ 10^{-4}\ |A_e|^2 .$$

Hence

$$\frac{P_r}{P_i} \approx \frac{.37}{R^2} .$$

The above relation if it is included with the field due to the continuous radiation, have been plotted (Theoretical Maley - Chang) in Figure 27. It may be argued that the discrepancy between the theoretical curves and the experimental is excessive. This is felt to be caused by the fact that the experimental result show the maximum magnitude of the electric field inside the curved waveguide is shifted toward the outside slab boundary indicating that there are additonal modes present that are not taken into consideration in the theoretical analysis. These have the effect of increasing or decreasing the magnitude of the electric field, depending whether they interfere constructively or destructively, and hence the measurements are not exactly comparable with the theory which assumes the field inside the slab behaves similar to that in the straight one except for a small shift toward the outside slab surface due to the Airy function behavior inside the curved waveguide. This can be seen from equation 2-34, if we replace the exponential term by a linear profile $n(1 + \frac{2x}{R})$ since the variation of x is small inside the slab. The solution of this differential equation with a linear profile is an Airy function [21]. These theoretical analysis also do not take into consideration the inside region radiation in the curved structure due to the discontinuity. These radiations clearly have strong influence for small radius of curvature. As indicated in Figs. 23 and 24, on the

inner side of the curved slab, the electric field has a high order mode in addition to the fundamental one especially in the case $R = 60\lambda$; this can only be explained if there is some inside radiation due to the discontinuity from the straight waveguide into the curved one.

(c) Minimization of radiation at bends:

Chang [11], suggested that a refractive index having an $\frac{R}{\rho}$ dependence in the exterior region of the curved slab will completely eliminate the continuous radiation. Unfortunately this kind of profile is not physically possible since it requires the refractive index to vanish at infinity. However an inverse-linear profile truncated at some finite distance has the effect of reducing radiation. This can be achieved in a model by compressing a polyethylene foam slab of a larger initial volume and with a specific profile (like inverse-linear) into the required dimension, a higher refractive index with a linearly graded profile can be achieved [22].

With our experimental set up, it was very hard to accomplish this type of linearly graded profile because it requires strong forces on the top and the bottom of the two parallel plates. Also there is difficulty in keeping the rectangular shape of the slab, since a pressure from the top and bottom will increase the width of the slab (a bulging effect). Finally it was decided to use a curved slab with a 1λ width

having trapezoidal (.95 cm and .55 cm in thickness) or triangular shape added to the outside boundary of a 1.7λ curved rectangular slab (.95 cm in thickness). The two sections were joined together to form a trapezoidal dielectric waveguide with a 2.7λ in width, as shown in Fig. 25. The assumption was that the refractive index in these trapezoidal sections would have the effect of averaging out with the air region and hence providing a truncated inverse-linear profile. Interestingly enough, for the same type of configuration as in part b of this Chapter, the radiation in the outside region dropped by the amount of 3 db due to this kind of tapering. Figures 25 and 26 give the magnitude and phase of the radial transverse field distribution for a fixed radius of curvature R = 90λ with no tapering and with the trapezoidal and triangular type profile on the outside region of the curved slab. It is clear from the magnitude curves that there is a decrease in radiation. It is also observed from Fig. 27 that the relative maximum of the electric field for a tapered type curved slab divided by the maximum electric field inside the straight slab is greater than for the experiment without the outer tapered section around the bend.

(d) Far field measurements

S. Maley [12], derived a far field pattern for a curved structure between two discontinuities. He made the assumption that the field propagates around the bend essentially

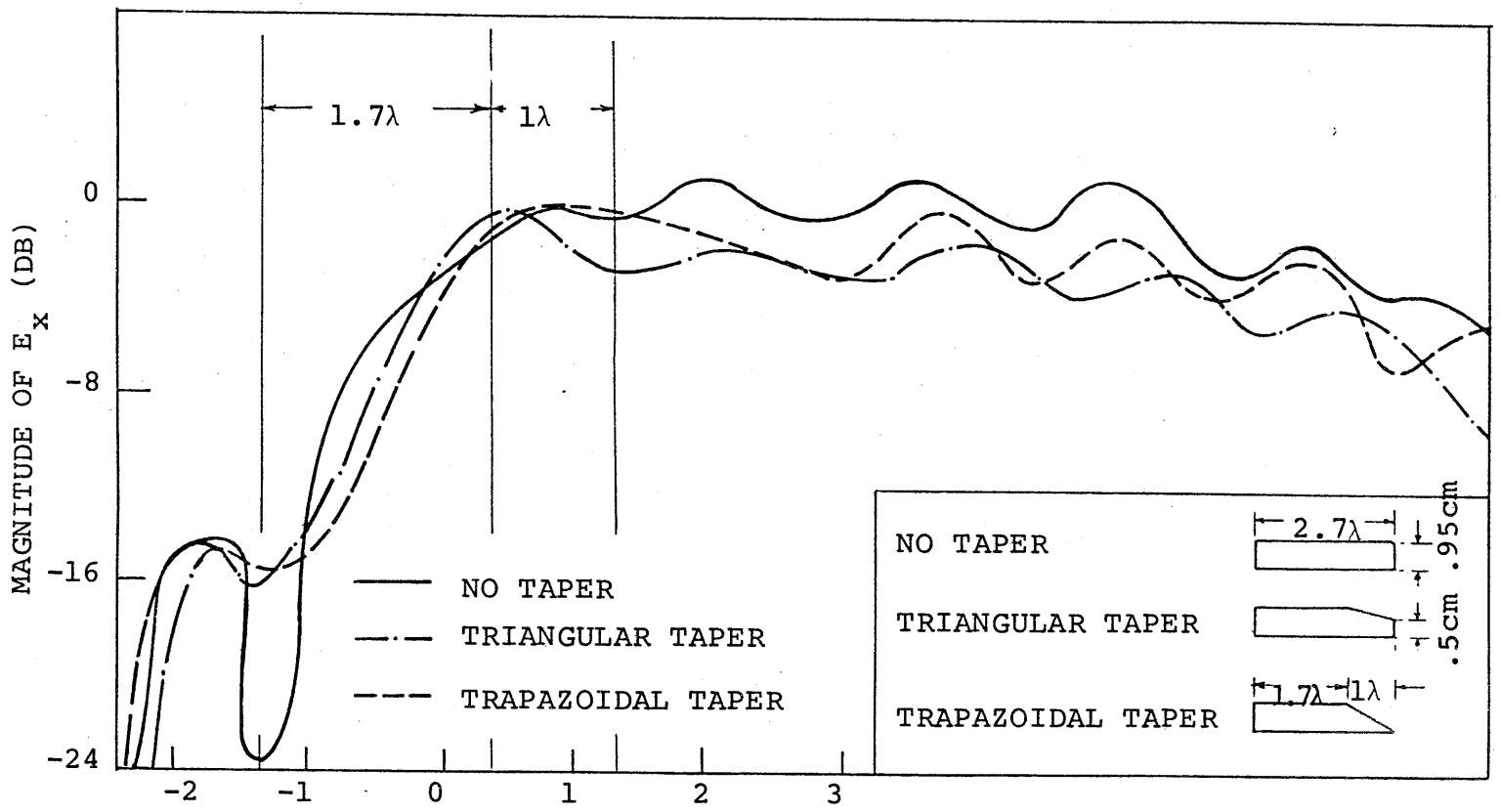

RADIAL DISTANCE IN WAVELENGTH
λ =3.3cm
For R = 90λ, ψ= 38°

Fig. 25 Magnitude of the Transverse Electric Field Vs. Radial distance with no tapering and with trapazoidal and triangular tapering for a fixed radius of curvature R = 90λ

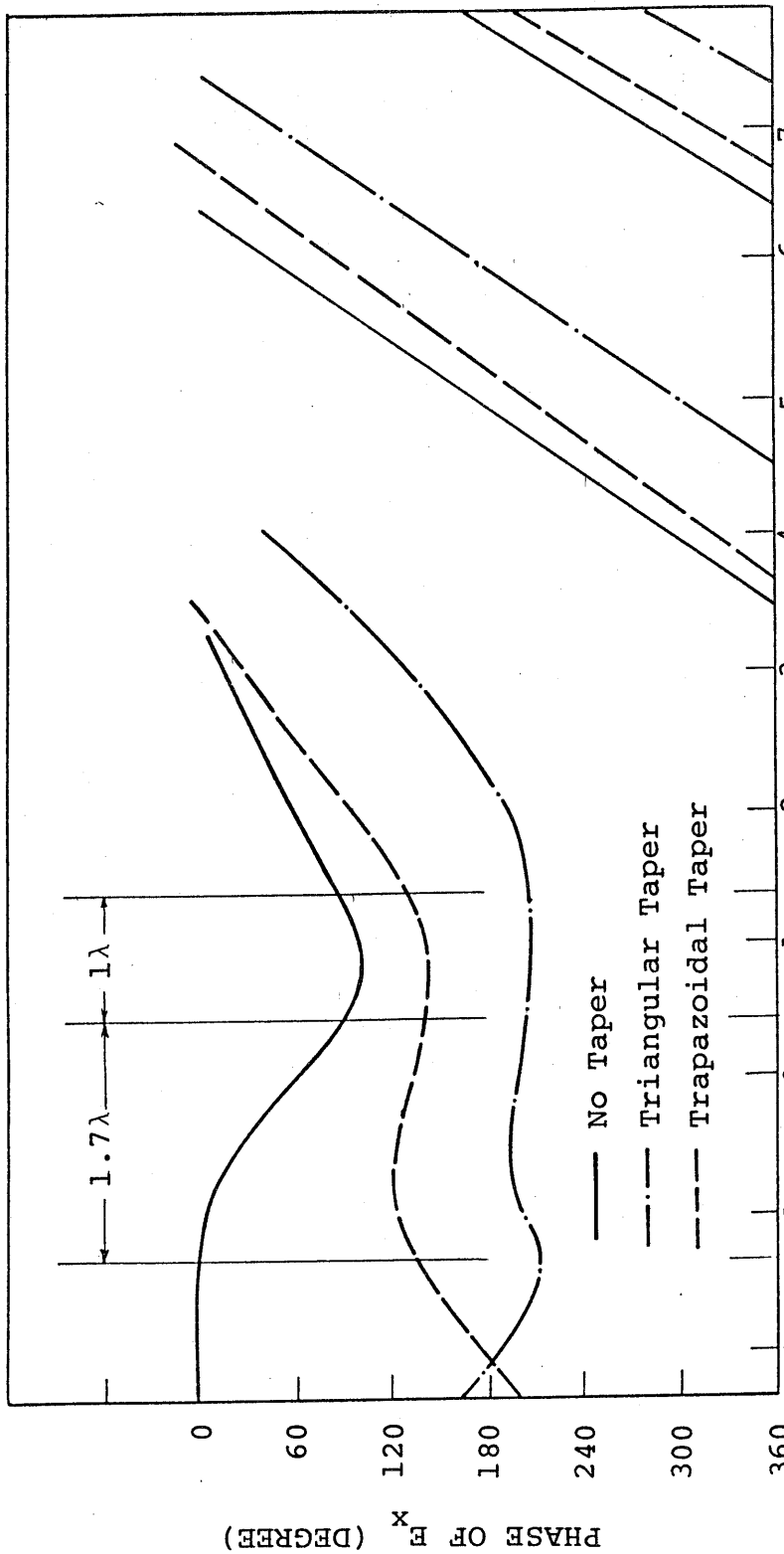

Fig. 26. Phase of the Transverse Electric Field shown in Fig. 25 Vs. Radial Distance

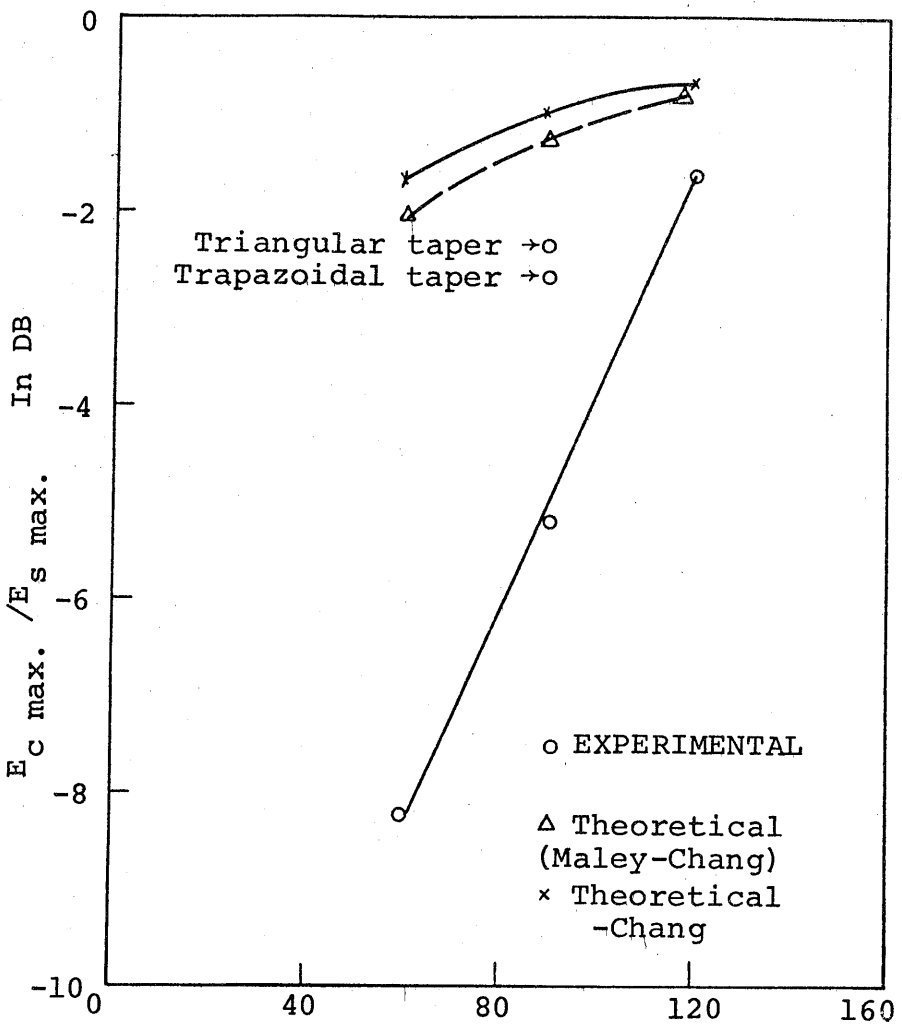

Fig. 27 The Max. Amplitude of the Transverse Electric Field of the Curved Section relative to the Max. Amplitude of the straight section Vs. the Radius of Curvature

unchanged compared to the straight waveguide. Also the observation point is so far away that the vectors R_1, R and R_3 (all shown in Fig. 5) become nearly parallel. Other approximations were made in evaluating the electric and magnetic potential function by using the asymptotic form for the Hankel function. The reason for these approximations was to get a closed form for the field pattern. An approximate number of lobes between the vertical and the waveguide was derived. It was shown that this number depends linearly on the radius of curvature and on the angle between the two straight guides as given in eq. 2-45.

To make a qualitative comparison with the theoretical analysis, radial transverse field measurements were made outside the curved slab at a larger angle (from the straight guide of region 1) than that given in part b of this chapter. Due to the limitation in the amount of space available for these measurements, we can not assume these plots as exactly far field data since they were measured close to the waveguide. Therefore the theoretical assumption that R_1, R and R_3 becomes parallel does not apply for this case of measurements. The number of lobes measured along the radial direction to the vertical are given in the following table for the theoretical (Eq. 2-45) and experimental results. In making this measurement, the field closer than 5 wavelengths from the outer surface of the waveguide was disregarded.

TABLE III

Radius of Curvature	ψ angle in degree	Number of lobes Experiment	Theory
90λ	38°	11	9
120λ	28°	5	4

Reasonable agreement can be seen even though the theory was derived for far field patterns. Figures 28 and 29 show the nearly Field Pattern measurements. The lobes look nearly equal in magnitude and closely spaced as was predicted by Maley [12].

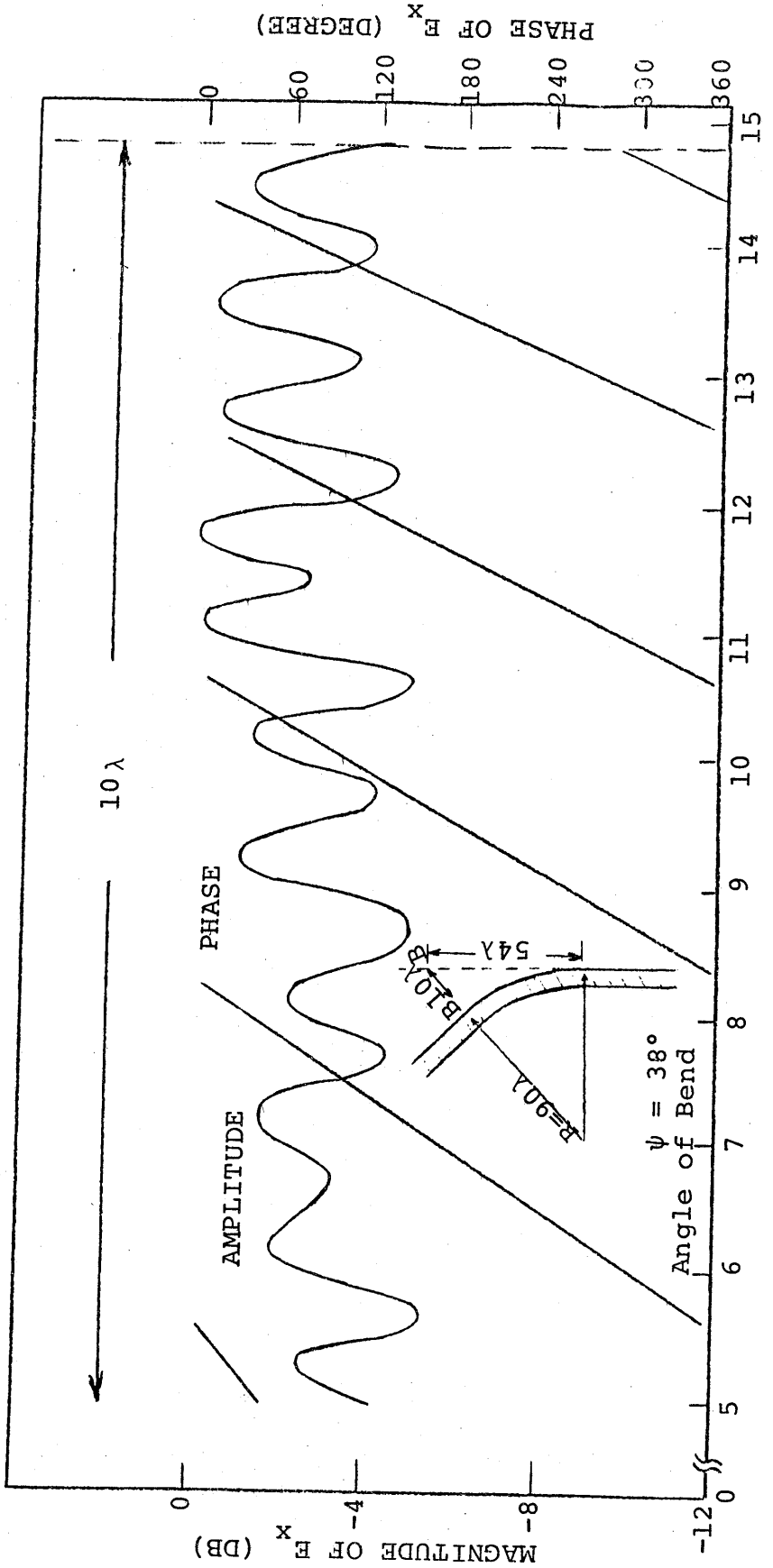

Fig. 28 Magnitude and Phase of the Transverse Electric Field Vs. Radial distance at the B-B section for R = 90λ and ψ = 38°

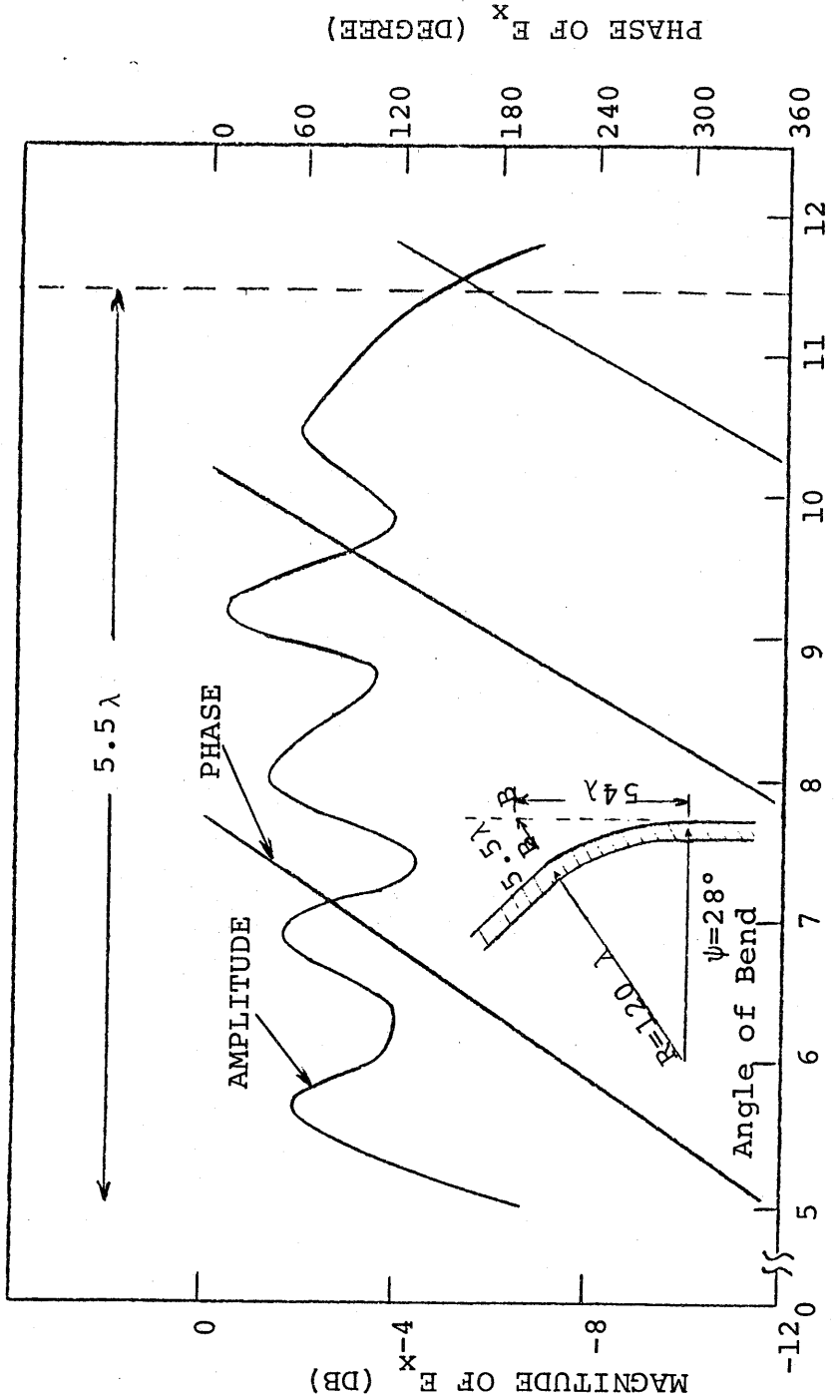

Fig. 29 Magnitude and Phase of the Transverse Electric Field Vs. Radial Distance at the B-B section for R = 120λ and ψ=28°
λ = 3.3cm

CHAPTER VII

CONCLUSIONS

We have presented a variety of experimental investigations dealing mainly with straight and curved dielectric slab waveguides. The design of the single straight slab was to insure single surface wave mode excitation and to have a tightly bound field (i.e., far above cutoff). The relative dielectric constant of the waveguide was about 1.03 at 9 GHz as was measured in previous experimental investigation (see Bahar [22].

There was a negative effect resulting from the use of the large horn for the excitation of the dielectric waveguide. Some of the radiation that flared from that large horn did not enter the dielectric waveguide. This external radiation influenced the measurements of the surface wave mode. Additional problems resulted from the large size of the two parallel plates and the consequent difficulty of moving them and of keeping them parallel.

The coupling between two waveguides was investigated theoretically and experimentally and it was shown that in the non-degenerate case the coupling length was less than that in the degenerate case and that complete power transfer cannot be achieved. As the separation between the two slabs was decreased, the coupling length decreased also. These results agree with theory.

Radial transverse electric field measurements were made

inside and outside the slab on a circular bend. These results indicate strong radiation due to the discontinuity from the straight slab into the curved one and also due to the continuous radiation from the bend. The influence of the radius of curvature was also investigated. It was found that radiation increases with a decrease in radius. This is also in agreement with theory. Reduction of radiation by using triangular and trapazoidal tapering in the cross sectional shape of the waveguide was also investigated and it was found that radiation could be reduced. Qualitative agreement was achieved between the theoretical derivation and experimental measurements for the number of lobes in the principal region of radiation of a bend. However, the measurements were not in the far field, due to size limitations imposed by the physical model.

REFERENCES

1. Kapany, N. S. and Burke, J. J., Optical Waveguide, New York: Academic Press, 1972.

2. Marcuse, Dietrich, Integrated Optics, IEEE Press, 1973.

3. Chang, D. C. and Kuester, E, "Lecture Notes in Optical Communication," Summer, 1974, to be published.

4. Marcuse, Dietrich, "The coupling of degenerate modes in two parallel dielectric waveguides," Bell Syst. Tech. J. 50, pp 1791-1816, 1971.

5. Maley, S. W. Chang, D. C. and Haddad, H., "Radiation from a Bend in a Dielectric Slab Waveguide, URSI Digest No. 10-7, p 178, 1974.

6. Chang, D. C., Maley, S. W., Barnes, F. S. and Haddad, H, "Energy Containment in Curved Sections of Dielectric Waveguide," URSI Digest, No. 10-8, p 178, 1974.

7. Collin, R., Field Theory of Guided Waves, McGraw-Hill, Chap. II, 1960.

8. Kuester, E. and Chang, D. C., "Non-degenerate surface-wave mode coupling of a system of dielectric waveguides," Electromagnetic Lab., University of Colorado, No. 9, October, 1974, to be published.

9. Von Hippel, A. R., Dielectrics and Waves, John Wiley & Son, N. Y., 1954.

10. Wait, J. R. and Bahar, E., "Simulation of curvature in a straight model waveguide," Electronic Letters, vol. 2, No. 10, p 358, March, 1966.

11. Chang, D. C. and Barnes, F. S., "Reduction of Radiation Loss in a Curved Dielectric Slab Waveguide," Electromagnetic Lab., University of Colorado, No. 2, July, 1973, to be published.

12. Maley, S. W., "Radiation from a Circular Bend Between Two Discontinuities in a Dielectric Slab Waveguide," Electromagnetic Lab., University of Colorado, No. 10. December, 1974, to be published.

13. Arnaud, J. A., "Transverse Coupling in Fiber Optics, Part I: Coupling between Trapped Modes," The Bell System Technical vol. 53, No. 2, p 217, February, 1974.

14. Jones, A. L., "Coupling of Optical Fibers and Scattering in Fibers," Journal of The Optical Society of America, vol. 55, No. 3, p 261, March, 1965.

15. Maractili, E.A.J., "Bends in Optical Dielectric Guides," Bell System Technical Journal, p 1203, September, 1969.

16. Marcuse, D., "Bending Losses of the Asymmetric Slab Waveguide," Bell Syst. Tech. J., vol. 50, No. 8, p 2551, October, 1971.

17. Lewin, L., "Radiation from Curved Dielectric Slabs and Fibers," MTT, vol. 22, No. 7, p 718, July, 1974.

18. Neumann, E. G. and Rudolph, H. D., "Radiation from Bends in Dielectric Rod Transmission Lines, vol. MTT-23, No. 1, January, 1975.

19. Wait, J. R., "On Surface Wave Propagation Around a Bend," Acta Physica, Australia 32, p 113, 1970.

20. Budden, K. G, "Radio Waves in the Ionosphere," Cambridge Press, London.

21. Bahar, E., "Inhomogeneous dielectric filling to simulate curvature in model Earth-ionosphere Waveguide," Proc. IEE, vol. 116, No. 1, January, 1969.

23. Kerrigan, M., "On the Microwave Model Study of VLF Propagation in the Earth-ionoshphere Waveguide," Master Thesis, C.U., 1969.

24. Goubau, G., "Single-conductor surface-wave transmission lines," Proc. I.R.E., pp 619-624, June, 1951.

25. Barlow, H. and Cullen, A., "Surface Waves," Radio Section, Paper No. 1482, p 329, 1953.

26. Meyerhoff, A., "Interaction Between Surface-Wave Transmission Lines," Proc. I.R.E., p 1061, September, 1952.

27. Cullen, A., "The Excitation of Plane Surface Waves," Proc. IEE, vol. 101, part IV, pp 225-234, August, 1954.

28. Snitzer, E. and Osterberg, H., J. Opt. Soc. Am., p 499, vol. 51, (1961).

29. Snitzer, E., "Cylindrical Dielectric Waveguide Modes," J. Opt. Soc. Am., vol. 51, 1961.

30. Kapany, N. and Burke, J., J. Opt. Soc. Am., vol. 51, p 1067, 1961.

31. Snyder, A., J. Opt. Soc. Am., vol. 56, p 601, 1966.

32. Miller, S., "A Survey of Integrated Optics," IEEE J. Quantum Electronics, vol. 8, part 2, pp 199-205, February 1972.

33. Marcuse, D., Light Transmission Optics, New York, Van Nostrand Reinhold, Chapter 8, 1972.

APPENDIX

To solve for the transverse propagation constant inside the dielectric slab by finding the roots of the transcendental equation.

```
0010 PRINT "WAVEGUIDE PERMITTIVITY =";
0020 INPUT E2
0030 PRINT "PERMITTIVITY OF THE EXP. DECAY REGION=";
0040 INPUT E1
0050 PRINT "HALF WIDTH OF SLAB =";
0060 INPUT T
0070 LET U=188*T
0080 DEF FNY(X)=X*X*(TAN(X)*TAN(X)+1)-(E2-E1)*U*U
0090 PRINT "LOWER LIMIT,UPPER LIMIT,STEP=";
0100 INPUT I,J,K
0110 PRINT
0120 FOR X=I TO J STEP K
0130   LET Y=FNY(X)
0140   LET X3=X
0150   IF Y=0 GOTO  0250
0160   IF Y>1E+35 GOTO  0280
0170   IF X=I GOTO  0200
0180   IF Y1=0 GOTO 0200
0190   IF SGN(Y)<>SGN(Y1) GOTO  0300
0200   LET X1=X2
0210   LET Y1=FNY(X1)
0220   PRINT X,Y
0230 NEXT X
0240 END
0250 PRINT "THERE IS A ROOT AT ";
0260 PRINT X3
0270 GOTO 0200
0280 PRINT "THERE IS A POLE AT";
0290 GOTO 0260
0300 REM     ---BISECTION
0310 LET X2=X
0320 LET Y2=Y
0330 LET X3=(X1+X2)/2
0340 LET Y3=FNY(X3)
0350 IF SGN(Y1)<>SGN(Y3) GOTO 0400
0360 LET P=ABS(Y3)-ABS(Y1)
0370 LET X1=X3
0380 LET Y1=Y3
0390 GOTO 0430
0400 LET P=ABS(Y3)-ABS(Y1)
0410 LET X2=X3
0420 LET Y2=Y3
0430 REM    ---CONVEREGENCE
0440 IF ABS(X2-X1)<1E-35 GOTO 0470
0450 IF ABS(X2-X1)<.000001*ABS(X1) GOTO 0470
0460 GOTO 0330
0470 IF P>0 GOTO  0280
0480 GOTO 0250
```

To find the relative magnitude and phase of the transverse electric field in the second waveguide with respect to the first (excited guide) for degenerate surface wave mode.

```
0010 INPUT L,E
0020 PRINT
0030 PRINT "EPSILON=";E
0040 PRINT
0070 FOR I=1 TO 3
0080   READ D,G1
0090   LET K0=188.626
0100   LET B=0
0110   LET Q1=(-B+G1)/D
0120   LET Q=(-B+G1)/(-B-G1)
0130   LET G=K0*G1*L
0140   LET A1=SQR(((1-Q)*COS(G))↑2+((1+Q)*SIN(G))↑2)
0150   LET A2=2*Q1*SIN(G)
0160   LET A=8.6859*LOG(A2/A1)
0170   LET P1=ATN((-B/G1)*TAN(G))
0180   LET P=180*P1/(4*ATN(1))
0190   PRINT "AMP.=";A,"PHASE=";P
0200 NEXT I
0210 DATA  1.45502E-3, 1.45502E-3
0220 DATA  1.12294E-3, 1.12294E-3, 8.66655E-4, 8.66655E-4
0230 END
```

To find the relative magnitude and phase of the transverse electric field in the second waveguide with respect to the first (excited guide) for non-degenerate surface wave mode.

```
0010 INPUT L,E
0020 PRINT
0030 PRINT "EPSILON=";E
0040 PRINT
0050 LET B1=1.0136
0060 LET B2=1.0087
0070 FOR I=1 TO 3
0080   READ D,G1
0090   LET K0=188.626
0100   LET B=.5*(B1-B2)
0110   LET Q1=(-B+G1)/D
0120   LET Q=(-B+G1)/(-B-G1)
0130   LET G=K0*G1*L
0140   LET A1=SQR(((1-Q)*COS(G))↑2+((1+Q)*SIN(G))↑2)
0150   LET A2=2*Q1*SIN(G)
0160   LET A=8.6859*LOG(1.089*A2/A1)
0170   LET P1=ATN((-B/G1)*TAN(G))
0180   LET P=180*P1/(4*ATN(1))
0190   PRINT "AMP.=";A,"PHASE=";P
0200 NEXT I
0210 DATA  2.03161E-3, 3.05742E-3
0220 DATA  1.53433E-3, 2.81708E-3, 1.15877E-3, 2.66927E-3
0230 END
```

To calculate the attenuation constant α due to the continuous radiation from a bend.

```
0010 INPUT R
0020 PRINT
0030 PRINT "RADIUS OF CURVATURE=";R
0040 LET E=1.03
0050 LET B=1.00939
0060 LET K0=188.626
0070 LET D=.092
0080 LET L=SQR(B*B-1)
0090 LET M=SQR(E-B*B)
0100 LET L1=D*2/(K0*L)
0110 LET T=2*K0*L*(B*R-R-D)/3
0120 LET F1=L*M*M/((E-1)*B*L1)
0130 LET F2=EXP(-2*K0*R*L*L*L/(3*B*B))
0140 LET F3=F1*F2
0150 PRINT "ALPHA-CHANG =";F3
0160 LET P=4*ATN(1)
0170 LET G1=K0*M*M*SQR(P*L/(K0*R))/(2*B*B*B*(E-1))
0180 LET G=G1*F2
0190 PRINT "ALPHA-LEWIN =";G
0200 GOTO 0010
0210 END
```

To calculate the total radiated power from a circular bend between two discontinuities.

```
0010 LET P=4*ATN(1)
0020 FOR R=2 TO 4 STEP 1
0030   LET T=1.0033/R
0040   LET B=1.00939
0050   LET T1=SIN(2*T)
0060   LET L=SQR(B*B-1)
0070   LET A=COS(T)
0080   LET L1=B*B-A*A
0090   LET L2=L1*L1
0100   LET L3=L1*L1*L1
0110   LET B1=B*B-1
0120   LET A1=1/TAN(T)
0130   LET B2=B1*B1
0140   LET B3=B1*B1*B1
0150   LET A2=COS(T)*COS(T)
0160   LET A3=B*B
0170   LET H1=T1/(3*B1*L1)
0180   LET H2=((3*A3+A2)/L2+5*A3/(B1*L1)+(11*A3+4)/(2*B2))
0190   LET H3=(B*(2*A3+3)/(B3*L))*(3*P/2-ATN(L*A1/B))
0200   LET K1=H1*H2+H3
0210   LET K2=(-2/3)*(A*(3*A3+A2)/L3+(3*A3-1)/B3)
0220   LET G1=(T1/(3*L1))*(-(3*A3+A2)/L2+A3/(B1*L1)+(A3+2)/(2*B2))
0230   LET G2=(B/(B2*L))*(3*P/2-ATN(L*A1/B))
0240   LET K3=G1+G2
0250   PRINT "K1 =";K1,"K2 =";K2,"K3 =";K3
0260   PRINT H1,H2,H3,G1,G2
0270 NEXT R
0280 END
```